ISSN 2587-1366

TUJE

# TURKISH JOURNAL OF ENGINEERING

VOLUME 1 ISSUE 1 MAY 2017

## TURKISH JOURNAL OF ENGINEERING (TUJE)

Turkish Journal of Engineering (TUJE) is a multi-disciplinary journal. The Turkish Journal of Engineering (TUJE) publishes the articles in English and is being published 3 times (January, May, September) a year. The Journal is a multidisciplinary journal and covers all fields of basic science and engineering. It is the main purpose of the Journal that to convey the latest development on the science and technology towards the related scientists and to the readers. The Journal is also involved in both experimental and theoretical studies on the subject area of basic science and engineering. Submission of an article implies that the work described has not been published previously and it is not under consideration for publication elsewhere. The copyright release form must be signed by the corresponding author on behalf of all authors. All the responsibilities for the article belongs to the authors. The publications of papers are selected through double peer reviewed to ensure originality, relevance and readability.

## AIM AND SCOPE

The Journal publishes both experimental and theoretical studies which are reviewed by at least two scientists and researchers for the subject area of basic science and engineering in the fields listed below:

Aerospace Engineering
Environmental Engineering
Civil Engineering
Geomatic Engineering
Mechanical Engineering
Geology Science and Engineering
Mining Engineering
Chemical Engineering
Metallurgical and Materials Engineering
Electrical and Electronics Engineering
Mathematical Applications in Engineering
Computer Engineering
Food Engineering

## PEER REVIEW PROCESS

All submissions will be scanned by iThenticate® to prevent plagiarism. Author(s) of the present study and the article about the ethical responsibilities that fit PUBLICATION ETHICS agree. Each author is responsible for the content of the article. Articles submitted for publication are priorly controlled via iThenticate ® (Professional Plagiarism Prevention) program. If articles that are controlled by iThenticate® program identified as plagiarism or self-plagiarism with more than 25% manuscript will return to the author for appropriate citation and correction. All submitted manuscripts are read by the editorial staff. To save time for authors and peer-reviewers, only those papers that seem most likely to meet our editorial criteria are sent for formal review. Reviewer selection is critical to the publication process, and we base our choice on many factors, including expertise, reputation, specific recommendations and our own previous experience of a reviewer's characteristics. For instance, we avoid using people who are slow, careless or do not provide reasoning for their views, whether harsh or lenient. All submissions will be double blind peer reviewed. All papers are expected to have original content. They should not have been previously published and it should not be under review. Prior to the sending out to referees, editors check that the paper aim and scope of the journal. The journal seeks minimum three independent referees. All submissions are subject to a double blind peer review; if two of referees gives a negative feedback on a paper, the paper is being rejected. If two of referees gives a positive feedback on a paper and one referee negative, the editor can decide whether accept or reject. All submitted papers and referee reports are archived by journal Submissions whether they are published or not are not returned. Authors who want to give up publishing their paper in TUJE after the submission have to apply to the editorial board in written. Authors are responsible from the writing quality of their papers. TUJE journal will not pay any copyright fee to authors. A signed Copyright Assignment Form has to be submitted together with the paper.

## PUBLICATION ETHICS

Our publication ethics and publication malpractice statement is mainly based on the Code of Conduct and Best-Practice Guidelines for Journal Editors. Committee on Publication Ethics (COPE). (2011, March 7). Code of Conduct and Best-Practice Guidelines for Journal Editors. Retrieved from http://publicationethics.org/files/Code%20of%20Conduct_2.pdf

## PUBLICATION FREQUENCY

The TUJE accepts the articles in English and is being published 3 times. January, May, September a year.

## CORRESPONDENCE ADDRESS

Journal Contact: tuje@mersin.edu.tr

# CONTENTS

## *Volume 1 – Issue 1*

## ARTICLES

# Turkish Journal of Engineering

*Turkish Journal of Engineering (TUJE)*
*Vol. 1, Issue 1, pp. 1-4, May 2017*
*ISSN 2587-1366, Turkey*
*DOI: 10.31127/tuje.315227*
*Research Article*

## CARBONATION RESISTANCE OF SLAG MORTARS ACTIVATED BY DIFFERENT ALKALI ACTIVATORS

Cahit Bilim *[1] and Cengiz Duran Atiş [2]

[1] Mersin University, Engineering Faculty, Department of Civil Engineering, Mersin, Turkey
(cbilim@mersin.edu.tr)

[2] Erciyes University, Engineering Faculty, Department of Civil Engineering, Kayseri, Turkey
(cdatis@erciyes.edu.tr)

* Corresponding Author
Received: 03/04/2017 Accepted: 29/04/2017

**ABSTRACT**
In this study, the carbonation depths of slag mortars activated by sodium silicate (water glass), sodium hydroxide and sodium carbonate were investigated and the results were compared to those of control mortar with CEM I 42.5 R normal Portland cement. In the mixture, the sand/binder ratio was 2.75 and the water/binder ratio was 0.50. Na concentrations in the mixture proportions were determined as 4%, 6%, and 8% for all the activators. For liquid sodium silicate activator, $SiO_2/Na_2O$ ratios (Ms) of 0.75, 1, 1.25, and 1.5 were also chosen. Prismatic specimens having 40 x 40 x 160 mm dimensions were prepared from both fresh Portland cement and slag mortar mixtures for the measurements. The day after the mortar casting, the prisms were demolded and placed in a humidity cabinet at 65% ± 5 relative humidity and 22 ± 2 °C temperature. The carbonation tests of mortars were conducted at 7, 28, 90 and 180 days. It was observed that the carbonation resistance of slag mortars activated by alkalis was lower than that of control mixture with Portland cement. However, it was also seen that an increment in the Na dosage of activator improved the resistance of the activated slag mortars to carbonation.

***Keywords:*** *Carbonation, Mortar, Slag, Activator*

## 1. INTRODUCTION

The use of mineral admixtures in today's concrete technology has an important place because of the positive effects on strength and durability of concrete as well as reducing production costs. One of these mineral admixtures is the ground granulated blast furnace slag (GGBFS) which is by-product of the iron-steel industry. GGBFS consists mainly of lime and calcium–magnesium aluminosilicates and has the glassy granular structure which is formed when the molten blast-furnace slag is rapidly chilled by immersion in water (Erdoğan, 2010; Atiş *et al*., 2009)

GGBFS, which is exhibiting pozzolanic properties when finely ground, is used in the production of slag cement in cement industry or in the production of concrete containing mineral admixture by replacing it with ordinary Portland cement (OPC). However, the low early strength seen in slag-added concrete limits the use of such binder due to the slow rate of hydration. For this reason, a number of researches which can speed up reactions by increasing the rate of this low hydration have been carried out. The studies have shown that when the slags are activated with alkali activators, they can bring about a strong paste structure that can be used in construction applications and thus provide high strength by solving the low early strength problem (Collins and Sanjayan, 1999).

Various studies on alkali-activated slag (AAS) showed that these binders exhibited superior performance even in aggressive environments such as high temperature, chemical attack and freeze-thaw cycles in comparison to OPC (Palacios and Puertas, 2007; Neto *et al*., 2008; Bilim, 2016). Byfors *et al.* (1989) noted that AAS concrete had a higher carbonation rate compared to OPC concrete having the equivalent compressive strength grade. Bilim and Atiş (2012) studying on alkali activation of mortars containing different replacement levels of GGBFS reported that the carbonation depths for liquid sodium silicate-activated OPC/slag mortars were higher than OPC mortar. Bernal *et al*. (2010) reported that alkali-activated binders were, on the whole, highly resistant to carbonation contrary to some claims in the literature.

As seen in the literature, there are a lot of published papers about some properties of mortar containing AAS as the binder. However, there is no adequate information on the carbonation properties of AAS materials without OPC. Therefore, this study focuses on the investigating of carbonation properties of the slag mortars activated with some alkali activators such as liquid sodium silicate, sodium carbonate and sodium carbonate.

## 2. EXPERIMENTAL STUDY

The cement was ASTM Type I normal Portland cement (42.5 MPa) with a specific gravity of 3.16 g/cm$^3$ and a Blaine specific surface area of 325 m$^2$/kg. The chemical oxide composition is presented in Table 1. GGBFS was procured from the Iskenderun Iron–Steel Plant in Turkey. Its chemical composition is as shown in Table 1. The specific gravity of GGBFS was 2.81 g/cm$^3$ and its Blaine specific surface area was about 425 m$^2$/kg. Slag is classified as a category 80 in terms of hydraulic activity index according to the requirements of ASTM C 989 (1994). Sodium hydroxide and sodium carbonate (obtained from MERCK chemicals) and liquid sodium silicate (obtained from Mersin Sişecam Soda Factory) were used as activators. Liquid sodium silicate had a $SiO_2/Na_2O$ ratio (Ms) = 2. The natural sand with maximum size of 4 mm was used. The grading complied with the requirements of ASTM C 33 (2005). The absorption value of the sand was 1.2% and the relative density at saturated surface dry condition was 2.67.

Table 1 Chemical composition of OPC and GGBFS (%)

| Oxide | OPC | GGBFS |
|---|---|---|
| $SiO_2$ | 19.71 | 36.70 |
| $Al_2O_3$ | 5.20 | 14.21 |
| $Fe_2O_3$ | 3.73 | 0.98 |
| CaO | 62.91 | 32.61 |
| MgO | 2.54 | 10.12 |
| $SO_3$ | 2.72 | 0.99 |
| $K_2O$ | 0.90 | 0.76 |
| $Na_2O$ | 0.25 | 0.42 |
| LOI | 0.96 | - |

Three different concentrations of sodium were selected for the activation of the mortars, 4%, 6% and 8% by weight of the slag. Liquid sodium silicate and sodium hydroxide were mixed at different ratios to obtain four Ms values (0.75, 1.00, 1.25 and 1.50) in solution. In order to keep the ratio of water/binder of 0.50, the amount of water to be added to the mortar mixtures is decreased by considering the amount of water in the solution. A summary of the experimental program is presented in Table 2.

Table 2 Summary of the experimental program

| Mixture Name | Activator Type | Sodium Dosage |
|---|---|---|
| OPC Mortar | - | - |
| AAS Mortar | Sodium hydroxide | 4%,6%,8% |
| AAS Mortar | Sodium carbonate | 4%,6%,8% |
| AAS Mortar | Liquid sodium silicate (Ms=0.75, 1, 1.25, 1.5) | 4%,6%,8% |

Prismatic specimens having 40 x 40 x 160 mm dimensions were prepared from both fresh OPC and AAS mortar mixtures for the measurements. The day after the mortar casting, the prisms were demolded and placed in a humidity cabinet at 65% ± 5 relative humidity and 22 ± 2 °C temperature. The carbonation tests of mortars were conducted at 7, 28, 90 and 180 days.

The phenolphthalein method was used to watch the pH change of mortar specimens in carbonation experiments. The phenolphthalein indicator shows a magenta colored region on the concrete where the pH value exceeds about 9 and a colorless region at the originally exposed surface where carbonation has reduced the pH to below 9. At the time of measurement, a 1% phenolphthalein solution in alcohol was sprayed on a broken surface of the remaining mortar prisms from flexural strength test, and the depth of neutralization was measured. The values were expressed by taking the average of three prismatic specimens. The results of flexural and compressive strength for AAS mortars were earlier presented by Atiş *et al*. (2009).

## 3. RESULTS AND DISCUSSION

Carbonation is a durability problem that starts from the surface of the concrete and progresses to its interior. The most important process that needs to be done in order to prevent the carbonation which is important for the corrosion of the reinforcement is to produce the concrete as impermeable as possible.

The carbonation depths at 7, 28, 90 and 180 days for slag mortars activated by liquid sodium silicate (LNS) are given in Table 3. Table 3 also shows the carbonation values of OPC. Additionally, the results obtained from slag mortars activated by sodium hydroxide (NH) and sodium carbonate (NC) activators are presented in Table 4 and Table 5, respectively.

Table 3. Carbonation depth of slag mixes with LNS (mm)

| | Activator Type | Activator Dosage | 7 | 28 | 90 | 180 |
|---|---|---|---|---|---|---|
| Cement | — | — | 0.38 | 0.81 | 3.14 | 4.20 |
| Slag | LNS | 4% Na, Ms=0.75 | 0.25 | 2.15 | 7.14 | 12.25 |
| | LNS | 4% Na, Ms=1.00 | 0 | 1.74 | 6.50 | 11.69 |
| | LNS | 4% Na, Ms=1.25 | 0 | 1.35 | 5.27 | 8.59 |
| | LNS | 4% Na, Ms=1.50 | 0 | 1.09 | 4.73 | 7.78 |
| | LNS | 6% Na, Ms=0.75 | 0 | 0.58 | 3.96 | 5.26 |
| | LNS | 6% Na, Ms=1.00 | 0 | 0.29 | 3.39 | 6.35 |
| | LNS | 6% Na, Ms=1.25 | 0 | 0.21 | 2.93 | 5.90 |
| | LNS | 6% Na, Ms=1.50 | 0 | 0.14 | 1.66 | 4.34 |
| | LNS | 8% Na, Ms=0.75 | 0 | 0.50 | 1.85 | 4.30 |
| | LNS | 8% Na, Ms=1.00 | 0 | 0.35 | 0.71 | 3.63 |
| | LNS | 8% Na, Ms=1.25 | 0 | 0.25 | 0.53 | 2.33 |
| | LNS | 8% Na, Ms=1.50 | 0 | 0.18 | 0.40 | 1.78 |

Table 4. Carbonation depth of slag mixes with NH (mm)

| | Activator Type | Activator Dosage | 7 | 28 | 90 | 180 |
|---|---|---|---|---|---|---|
| Slag | NH | 4% Na | 0.13 | 1.73 | 3.92 | 7.76 |
| | NH | 6% Na | 0 | 1.41 | 3.04 | 5.59 |
| | NH | 8% Na | 0 | 0.90 | 2.04 | 3.09 |

Table 5. Carbonation depth of slag mixes with NC (mm)

| | Activator Type | Activator Dosage | 7 | 28 | 90 | 180 |
|---|---|---|---|---|---|---|
| Slag | NC | 4% Na | 0.26 | 4.04 | 10.47 | 17.80 |
| | NC | 6% Na | 0 | 3.04 | 6.31 | 10.18 |
| | NC | 8% Na | 0 | 2.25 | 5.62 | 9.25 |

The results show that an increase in the carbonation values of all mortars happened in time depending on the amount of $CO_2$ that permeates to the interior of specimen.

The highest carbonation values were obtained from the slag mortars activated by sodium carbonate activator due to calcium carbonate crystals that happens as a result of chemical reactions between $CO_3^{2-}$ ions in the structure of $Na_2CO_3$ and $Ca^{2+}$ ions coming from the slag.

Additionally, it is thought that there is a decrease in carbonation values with an increase in Na dosage, and this is probably due to the relatively higher level pH environment that occurs in the pore solution due to the increased Na dosage. Similarly, the rising silicate modulus (Ms) in the slag mortars activated with the sodium silicate solution produced the lower carbonation values.

From all the tables, it was seen that carbonation in AAS mortars had higher values compared to OPC mortar. This situation may be explained in this way: When AAS concretes are exposed to a carbon dioxide-rich medium, some chemical changes occur in the binder matrix such as the formation of calcium carbonate crystals, a decrease in the pH level of the pore solution, and a decomposition of the lime from the C-S-H gels. Because $Ca^{2+}$ content in the slag incorporated concretes is lower than OPC concrete, $CaCO_3$ precipitation is rare. So, the diffusion of $CO_2$ into the interior of the concrete is easier since the porosity increases in the area where the $CaCO_3$ crystals occurs dependent on the carbonation reaction. This situation leads to the faster advancing of the carbonation reactions from the surface towards to interior increasing the carbonation.

On the other hand, OPC concretes have more $Ca^{2+}$ content in comparison with AAS concretes. When the binder matrix comes into contact with $CO_2$, the $CaCO_3$ crystals precipitate in the pores, and thus produce a barrier which prevents the diffusion of $CO_2$ into the paste. Therefore, the carbonation reactions in OPC paste progress more slowly and the carbonation values of AAS concretes are higher than those of OPC concrete (Bilim, 2006).

The changes in the carbonation depths, which were measured over the 180-day time period for both OPC mortar and the slag mortars activated with different alkali activators, are shown in Fig. 1.

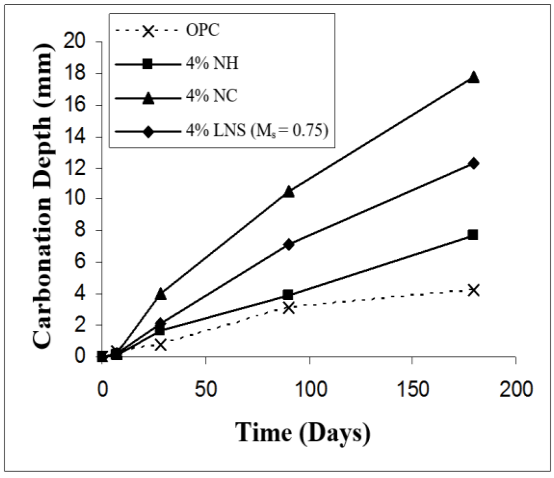


Fig. 1. The changes in carbonation depths of both OPC and AAS mortars

## 4. CONCLUSION

The following conclusions can be drawn from this study:

1. The findings obtained from the test results exhibited that the carbonation resistance of slag mortars activated by alkalis was lower than that of control mixture with OPC.
2. The highest carbonation values were obtained from the slag mortars activated by sodium carbonate activator.
3. An increment in the Na dosage of activator improved the resistance of the activated slag mortars to carbonation.
4. The rising silicate modulus (Ms) in the slag mortars activated with the liquid sodium silicate solution produced the lower carbonation values.

## REFERENCES

ASTM C 33 (2005). *Standard specification for concrete aggregates*, Annual Book of ASTM Standards, West Conshohocken, USA.

ASTM C 989 (1994). *Standard specification for ground granulated blast furnace slag for use in concrete and mortars*, Annual book of ASTM Standards, West Conshohocken, USA.

Atiş, C. D., Bilim, C., Çelik, Ö. and Karahan, O. (2009). "Influence of activator on the strength and drying shrinkage of alkali-activated slag mortar." *Construction and Building Materials*, Vol. 23, No. 1, pp. 548-555.

Bernal, S. A., Gutierrez, R. M., Provis, J. L. and Rose, V. (2010). "Effect of silicate modulus and metakaolin incorporation on the carbonation of alkali silicate-activated slags." *Cement and Concrete Research*, Vol. 40, No. 6, pp. 898–907.

Bilim, C. and Atiş, C. D. (2012). "Alkali activation of mortars containing different replacement levels of ground granulated blast furnace slag." *Construction and Building Materials*, Vol. 28, No. 1, pp. 708-712.

Bilim, C. (2016). "The fire resistance of alkali-activated slag mortars." *Çukurova University Journal of Engineering and Architecture*, Vol. 31, No. 2, pp. 67-75.

Bilim, C. (2006). The use of ground granulated blast furnace slag in cement based materials, PhD Thesis, University of Çukurova, Adana, Turkey.

Byfors, K., Klingstedt, V., Lehtonen, P. Y. Y. and Rombern, L. (1989). "Durability of concrete made with alkali activated slag." *Proc., 3rd International Conference on Fly Ash, Silica Fume, Slag and Natural Pozzolans in Concrete*, American Concrete Institute, Trondheim, Norway, pp. 1429-1466.

Collins, F. G. and Sanjayan, J. G. (1999). "Workability and mechanical properties of alkali activated slag concrete." *Cement and Concrete Research*, Vol. 29, No. 3, pp. 455-458.

Erdoğan, T. Y. (2010). *Concrete*, METU Press, Ankara, Turkey.

Neto, A. A. M., Cincotto, M. A. and Repette, W. (2008). "Drying and autogenous shrinkage of pastes and mortars with activated slag cement." *Cement and Concrete Research*, Vol. 38, No. 4, pp. 565-574.

Palacios, M. and Puertas, F. (2007). "Effect of shrinkage-reducing admixtures on the properties of alkali-activated slag pastes and mortars." *Cement and Concrete Research*, Vol. 37, No. 5, pp. 691-702.

# Turkish Journal of Engineering

*Turkish Journal of Engineering (TUJE)*
*Vol. 1, Issue 1, pp. 5-10, May 2017*
*ISSN 2587-1366, Turkey*
*DOI: 10.31127/tuje.316503*
*Research Article*

## ANALYSIS OF ANNUAL ENERGY REQUIREMENT OF A RESIDENTIAL HOUSE WITH TS825 AND ASHRAE HEAT BALANCE METHODS

Kaan Yaman [1] and Gökhan Arslan *[2]

[1] Mersin University, Engineering Faculty, Department of Mechanical Engineering, Mersin, Turkey
(yamankaaan@gmail.com)

[2] Mersin University, Engineering Faculty, Department of Mechanical Engineering, Mersin, Turkey
(garslan@mersin.edu.tr)

* Corresponding Author
Received: 28/03/2017 Accepted: 02/05/2017

**ABSTRACT**
Energy efficiency in buildings is an important up-to-date topic. For that reason, accurate calculation of heating and cooling loads is essential. In this study, heating and cooling loads of a residential house were determined by using national standards for different climatic zones Mersin, İstanbul, Ankara, Erzincan, and Erzurum. Calculations were performed by using the TS825 method that is based on national mandatory heat insulation standard TS825 and EnergyPlus software that is based on heat balance method. Heating loads obtained from simulations were compared on the monthly and annual basis. The absolute deviation between methods results was obtained in the range of 1.9 % to 39.5 %. The highest deviation was in Mersin where represents the 1st region and the lowest deviation was in Ankara where represents the 3rd region. Since TS825 method has not feature to simulate cooling load, annual cooling load calculated by using EnergyPlus software was 128.2 kWh/m$^2$y for Mersin, 70.7 kWh/m$^2$y for Istanbul, 44.9 kWh/m$^2$y for Ankara, 49.0 kWh/m$^2$y for Erzincan and 26.7 kWh/m$^2$y for Erzurum. Insufficiency of the TS825 method was examined in detail.

***Keywords:*** *Heating Load, Cooling Load, TS825, Heat Balance Method, EnergyPlus*

## 1. INTRODUCTION

Increasing population and industrialization in global scale lead to an increase in energy demand. Depletion of current energy resources and correspondingly increasing energy cost necessitate efficient consumption of energy resources. Buildings are one of the base energy consumption components and compose 20-40 % of the total energy consumption in worldwide (Perez-Lombard *et al.*, 2008). In the period of 2010-2014, buildings are averagely responsible for 35 % of the total energy consumption in Turkey according to the statistical report published by General Directorate of Energy Affairs (The Republic of Turkey, Ministry of Energy and Natural Resources, 2016). Despite the high energy consumption rate, buildings have energy saving potential. Developed countries attach particular importance to that potential and apply related regulations strictly. Due to a large number of old buildings and lack of inspection in regulation execution, energy consumption rate of buildings are high in Turkey. It is stated that only 16 % of buildings have a double glass window and insulated roof (Keskin, T., 2010). The most effective way of increasing energy efficiency is the energy saving applications. Since 1970, both standards and regulations have been developed to consume energy more efficiently and increase energy savings in Turkey. In this regard, a mandatory standard "TS825 Thermal Insulation Requirements for Buildings" was published in 2000 to increase savings in heating energy consumption rate of buildings. It is possible to save 25-50 % of energy consumption of buildings by only applying thermal insulation on building envelope (The Republic of Turkey, Ministry of Energy and Natural Resources, 2016).

Basically, accurate estimation of building energy demand without compromising on comfort conditions is required for building energy efficiency calculation. Experimental studies about the determination of building energy performance require high cost and long-term measurement period. For that reason, experimental measurement is rarely applied method in this field. In addition to that, high accuracy calculation method is a must to determine the energy demand of the building. Seasonal, hourly and dynamic calculation methods are used in building energy performance analysis. Simulation software codes are developed by using those methods to determine the energy demand of the building. In this study, TS825 method code developed base on seasonal calculation method and EnergyPlus® software developed base on dynamic calculation method are used. In that way, the energy demand of a single family house in different climatic regions of Turkey is calculated by using TS825 standard calculation method and heat balance method. Obtained results are used to compare methods with each other.

## 2. LITERATURE REVIEW

The simplest way of energy saving in buildings is the thermal insulation applications. By insulating the buildings, the required heating energy is decreased and energy saving is provided. Determining the correct material and optimum insulation thickness are very important issues in thermal insulation (Özkan, D. B., 2009). Required thermal insulation thickness differ according to the fuel type, climatic region, insulation material, window to wall ratio, etc. For all cities of Turkey, optimum insulation of thickness determined for two different fuels (natural gas, coal) and five different insulation material (rock-wool, glass-wool, XPS, EPS, polyurethane) (Kürekçi *et al.*, 2012). In those studies, the TS825 method was used and effect of methodology was not discussed in detail. Besides that, developed countries promote to form standards according to dynamic calculation procedure. ASHRAE heat balance method is referred as the most accurate approach to calculate the thermal loads in literature. EnergyPlus software algorithm was developed based on heat balance method. It is the official building simulation program of the United States Department of Energy, promoted through the Building and Technology Program of the Energy Efficiency and Renewable Energy Office. It is a widespread and accepted tool in the building energy analysis community around the world (Stadler *et al.*, 2006). Among the other simulation programs BLAST, BSim, DeST, DOE-2, ECOTECT, eQuest, ESP-r and TRNSYS, EnergyPlus program is defined as completely implemented for modelling characteristics such as simulation solution, time step approach, simultaneous radiation and convection, combined envelope heat and mass transfer, internal mass considerations, occupant comfort, solar gains, shading, and sky considerations (Harish and Kumar, 2015).

## 3. METHODOLOGY

In this study, villa type single family house placed in a rural area without any shading around is designed. Isometric view of the house is given in Fig. 1.

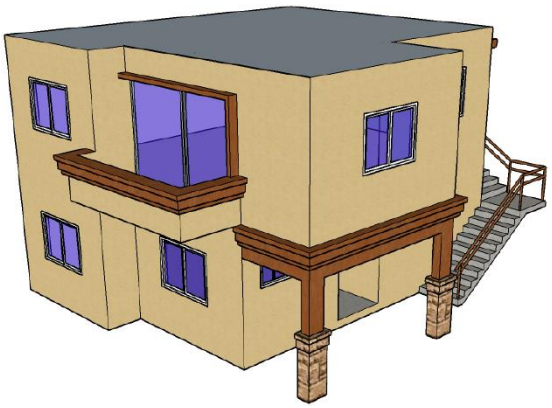

Fig. 1. Isometric view of the designed house

Designed house construction characteristics are designed to increase heat transfer rate. The rectangular form of the house is broken down by adding an overhang room and two balconies in the second floor. Story height of the house is 2.8 m and gross volume is 360.4 $m^3$. Outside wall surface area is 166.8 $m^2$ and window surface area is 28.3 $m^2$. The ratio of the glazing surface area to the outside wall surface area is 0.103 $m^2/m^2$ for the south facade, 0.038 $m^2/m^2$ for the north facade, 0.151 $m^2/m^2$ for the east facade, 0.380 $m^2/m^2$ for the west facade. Architectural plan of the house is given in Fig. 2.

Simulations were performed in different climatic regions of Turkey. Locations were determined by using heating degree-day (HDD). Accordingly, Ankara (annual

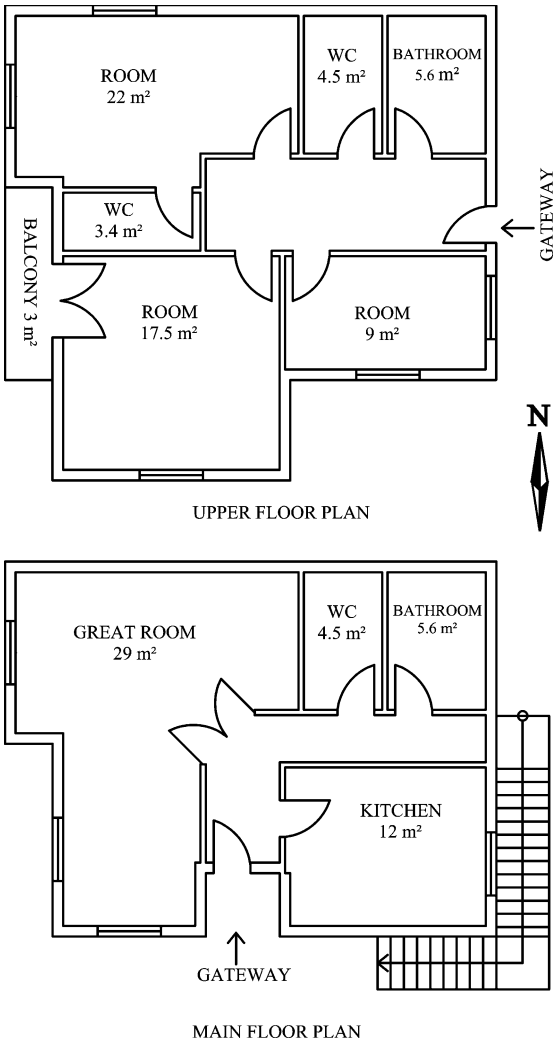


Fig. 2. Architectural plan of the house

HDD 2890), Erzincan (annual HDD 3157), Erzurum (annual HDD 4876), Istanbul (annual HDD 1714) and Mersin (annual HDD 1834) were selected.

In Table 1, overall heat transfer coefficients of the building envelope for different regions were given. Those values were determined in order to obey the maximum allowable values defined in TS825 standard (2013). For not changing the construction components for each location, U-values were modified by only increasing insulation thickness. Adding to that the weighted mean U-value of all components of building envelope was obtained. Mean U-values were 0.51 for Ankara, 0.45 for Erzincan, 0.38 for Erzurum, 0.57 for İstanbul and 0.64 for Mersin.

Table 1. Overall heat transfer coefficient (U) of building envelope

| Location | $U_{wall}$ | $U_{roof}$ | $U_{floor}$ | $U_{window}$ |
|---|---|---|---|---|
| Ankara | 0.42 | 0.28 | 0.42 | 1.80 |
| Erzincan | 0.34 | 0.23 | 0.37 | 1.80 |
| Erzurum | 0.27 | 0.15 | 0.29 | 1.80 |
| İstanbul | 0.48 | 0.32 | 0.50 | 1.80 |
| Mersin | 0.58 | 0.35 | 0.58 | 1.80 |

In this study, determination of the annual energy demand of the buildings that have a significant ratio in total energy demand is aimed at using the national standard TS825 method and heat balance method. To compare those methods, parameters such as building geometry, building envelope, heating-cooling setpoints, schedules, etc. should be the same for each one. At that point, it must be taken into account that TS825 calculation procedure requires seasonal average data and heat balance method requires hourly data. To minimize the input differences between two methods will clarify the sufficiency and applicability of the TS825 method. For that reason, details of the methods discussed in detail.

### 3.1. TS825 Method

In "TS825 Thermal Insulation Requirements for Buildings" standard (2013), only heating load calculation procedure was introduced. This method solves steady state heat conduction equation where required boundary conditions such as convection and solar gain are taken from the monthly average data table. Degree-day approach is used in the calculation procedure and 20 years average meteorological data is used. Turkey is divided into five climatic regions based on degree-day approach. According to that Mersin, Istanbul, Ankara, Erzincan, and Erzurum are selected where are placed in 1st, 2nd, 3rd, 4th and 5th regions, respectively. In the next step, the story height must be checked. Two different approaches are used according to the story height is above or below 2.6 m. To make the analysis more realistic, thermal bridges of the single family house introduced in heating load calculation procedure and given in Table 2. As a result, heating load is calculated by using Eq. (1).

$$Q_{TS} = [(H_T + H_v)(T_i + T_a) - \eta(F_i + F_s)]t \quad (1)$$

Here, $Q_{TS}$ represents heating load according to the TS825 method, $H_T$ is conduction heat transfer rate, $H_v$ is ventilation heat transfer rate, $T_i$ is the average zone air temperature, $T_a$ is the ambient air temperature, $\eta$ is monthly average usage factor, $F_i$ is internal heat gains and $F_s$ is the solar energy gains.

Table 2. Thermal bridges used in TS825 method

| Thermal bridge | Type* | Length, L (m) | Thermal conductivity, k (W/mK) |
|---|---|---|---|
| Balcony | B2 | 4.5 | 0.8 |
| Roof | R2 | 36.6 | 0.5 |
| Floor | F1 | 32.5 | 0.8 |
| Corner | C1 | 39 | 0.05 |
| Window | W8 | 59.9 | 0.6 |

***** The thermal transmittance type was determined according to TS EN ISO 14683 (2009).

### 3.2. Heat Balance Method

It is most widely used method by researchers due to its success in approximating heating-cooling loads. To apply this method to the designed single family house, EnergyPlus building energy simulation tool (V8.4) (U.S. Department of Energy, 2017) was used. This software algorithm was formed based on heat balance method in

which heat conduction, convection, and radiation equations are solved simultaneously in given timestep. The Conduction Transfer Function (CTF) algorithm is used which utilizes one-dimensional transient heat conduction through multilayers such as walls and floors. Comprehensive convection algorithm was used as Thermal Analysis Research Program (TARP) developed by Walton (Walton G.N., 1983). Heating load is calculated by using Eq. (2).

$$Q_{HB} = \left[h(T_i - T_s)\sum f_{s,s+1}(T_{s+1} - T_s)\right]A + Q_s + Q_l + Q_e \quad (2)$$

Here, $Q_{HB}$ represents heating load according to heat balance method, $h$ is convective heat transfer coefficient, $T_s$, $T_{s+1}$ are average temperature of interior surface "$s$" and "$s+1$", $f$ is linearized radiation heat transfer factor, $A$ is area of surface, $Q_s$ is the absorbed solar energy gains, $Q_l$ is the absorbed heat gain from lights sources and $Q_e$ is the absorbed heat gain equipment and occupants sources.

In this study, 15 minutes timestep was used EnergyPlus software requires a detailed hourly meteorological file of the region. TMY (Typical Meteorological Year) file is provided by using Meteonorm©. Heating and cooling load calculations are grouped under 6 different input data module.

- Simulation parameter inputs (heat balance algorithm),
- Regional and meteorological inputs,
- Scheduling input,
- Building construction detail input,
- Zone information input,
- Internal heat gains input.

Parameters required for load calculation used in those two methods are summarized in Table 3.

Table 3. Required parameters for determination of heating-cooling loads

| Parameters | Heat balance method | TS825 method |
|---|---|---|
| Comfort temperature | 19 °C (Heating)<br>23 °C (Cooling) | 19 °C (Heating) |
| Schedule | Weekdays 5 p.m. – 8 a.m.<br>Weekend 8 a.m. – 5 p.m. | |
| Ventilation | 0.7 $hr^{-1}$ Natural | 0.7 $hr^{-1}$ Natural |
| Lighting density | 200 W (compact fluorescence) | 5 $W/m^2$ (sum of whole internal heat gains) |
| Electric equip. | Refrigerator 80 W, LCD 100 W | |
| Other equip. | 50 W (Avg.) | |
| Occupancy | 0.03 Person/$m^2$ | |

### 3.3. Statistical Analysis

TS825 method and heat balance method were compared with statistical criteria proposed by ASHRAE Guideline 14 (2014). Simulated results were evaluated according to normalized mean bias error (NMBE) and coefficient of variation of the root mean square error (CVRMSE). These parameters were calculated by using Eqs. (3), (4), respectively.

$$NMBE = \frac{\sum_{i=1}^{n}(y_{HB,i} - y_{TS,i})}{n-1}\frac{100}{\bar{y}_{HB}} \quad (3)$$

$$CVRMSE = \left[\frac{\sum_{i=1}^{n}(y_{HB,i} - y_{TS,i})^2}{n-1}\right]^{1/2}\frac{100}{\bar{y}_{HB}} \quad (4)$$

Here, $y_{HB}$, $y_{TS}$ represent according to heat balance and TS825 methods, respectively. $n$ is the number of simulated value.

According to ASHRAE Guideline 14 (2014), acceptable tolerances for comparison of NMBE and CVRMSE are within ± 10 % and ± 30 %, respectively when monthly data considered.

## 4. RESULTS AND DISCUSSION

In this study, TS825 national standard and heat balance methods were compared to 5 different climatic regions of Turkey. Firstly, the single-family house was designed to meet all the criteria of TS825 national standard for all climatic regions. In Fig. 3, monthly heating loads obtained from those two methods was given. Acceptable tolerance defined in ASHRAE Guideline 14 was obtained only for Ankara (3$^{th}$ climatic region). Especially for the Mersin (1$^{st}$ climatic region) and Istanbul (2$^{nd}$ climatic region) CVRMSE and NMBE values are higher than the advisable limit. The main reason for this deviation is that local meteorological data was used in heat balance method and regional average meteorological data was used in the TS825 method. It is understood that 5 climatic region is not enough for accurate heating load calculations. Adding to that very low heating loads can be calculated in seasonal transition timeline in heat balance method but TS825 method results were overestimated the heating load at that timeline. The highest difference of calculated heating loads of the methods was obtained for Mersin in November as 3.8 kWh/$m^2$ and the lowest difference is obtained for Erzurum in June as 1.0 kWh/$m^2$.

In Fig. 4, comparison of calculated heating loads of the methods was done in annual base. The absolute deviation between methods results was obtained in the range of 1.9 % to 39.5 %. The highest deviation was in Mersin where represents the 1$^{st}$ region and the lowest deviation was in Ankara where represents the 3$^{rd}$ region. For other regions deviations were 11.5 % for Erzincan, 6.5 % for Erzurum, 20.8 % for Istanbul.

In Fig. 5, cooling load obtained in each region was given. Since the TS825 method is not including cooling load calculation procedure, only heat balance method results were given. The highest cooling load was obtained for Mersin where represents the 1$^{st}$ region.

The TS825 method assumes steady-state heat transfer and uses monthly average meteorological data. Heat balance method uses detailed hourly meteorological data. Since outside temperature and solar radiation data change hourly, this method obtained a dynamic solution.

The TS825 method includes 5 different degree-day regions. Outside air dry bulb temperature and solar radiation are assumed constant in a month with its average value for each region. Beside that EnergyPlus uses local and hourly meteorological data. When compared with EnergyPlus dynamic solution results, it is obvious that 5 degree-day regions are not adequate for a consistent solution.

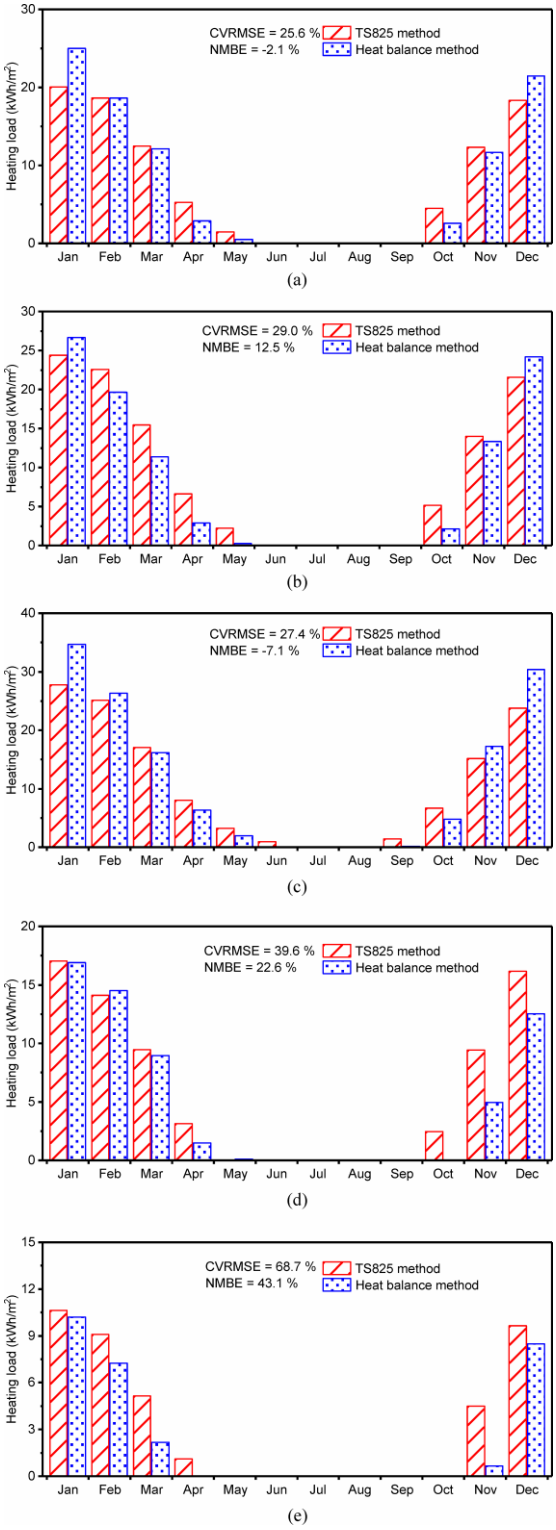


Fig. 3. Heating load on the monthly basis; (a) for Ankara; (b) for Erzincan; (c) for Erzurum; (d) for Istanbul and (e) for Mersin

The maximum allowable overall heat transfer coefficient defined for windows is $U_{window}$=1.8 W/m$^2$K in the TS825 method. However, in proposed study and practical applications, this criterion cannot be met. The double glazed window is used in this study and the overall heat

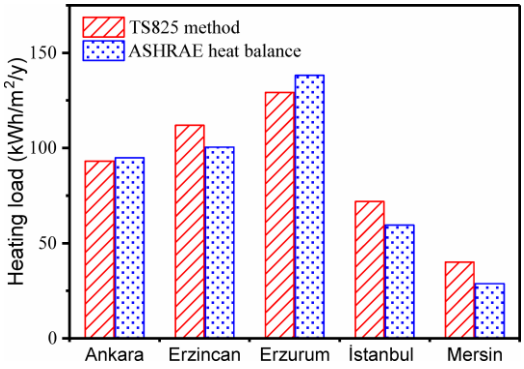


Fig. 4. Heating load on the annual basis

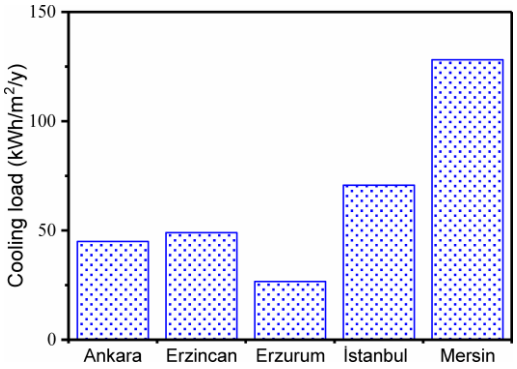


Fig. 5. Cooling load on the annual basis

transfer coefficient is 2.69 W/m$^2$K. In Table 1, construction components overall heat transfer coefficients were given. Glazing has the highest U-value and the most critical component in heating-cooling load calculations. For that reason, glazing total surface area must be determined logically. During daytime, the window provides solar energy heat gain for the building. Beside that higher U-value increases heat loss rate, windows behave like a black body at nights and that will increase heat loss rate, too. The TS825 method uses monthly average solar radiation that is perpendicular to windows surface area on calculation procedure of heating load. However, parameters such as geographical and solar angles are not included in that procedure. In heat balance method, solar gains and long wave solar radiation are solved by applying heat equations, separately. In calculation procedure of heating-cooling loads, solar gain is one of the most important environmental variable. For that reason, heat balance method is more accurate than the other methods.

Another important reason for the differences between the calculated thermal loads of the methods is that the TS825 method does not include the thermal mass calculations. In heat balance methods, energy storage in construction component is included in calculation procedure. By the way, faster cooling in the winter season and an extreme increase of inside temperature in the summer season will be prevented. This approach makes heat balance method more realistic.

The TS825 method only calculates the heating load. Since Mersin is placed in a hot climate region, cooling load is high. Simulation results showed that cooling load is three times higher than the heating load for Mersin. Proper insulation thickness determined according to

TS825 standard is also met required conditions for cooling load. Beside this, heating energy demand can be supplied in a wide range of sources but cooling energy demand is only supplied from electric energy. For that reason, calculation of cooling load accurately is important for energy efficiency.

In the TS825 method, zoning is done if only temperature difference is higher 4 °C between the building subdivisions. In heat balance method, control of zone via scheduling of occupancy, lighting intensity and electric equipment usage is optional. For that reason, simulation in Energy Plus is more realistic and more accurate.

HVAC systems designed based on this simulation program will be more suitable for capacity determination and energy consumption will decrease. In other words, the TS825 method can only be used for efficiency calculation of HVAC systems. Differently, HVAC systems can be designed by using the EnergyPlus software.

## 5. CONCLUSION

Buildings have a significant portion of total energy demand in both universal and national scales. Energy saving attempts will return buildings into an economic product. Accurate determination of building heating-cooling loads plays important role in energy saving studies. In this study, a national standard developed for building energy performance, the TS825 method was compared with heat balance method that was used in developed countries. A single-family house was analyzed for Mersin, Istanbul, Ankara, Erzincan, and Erzurum where represent the degree-day region from 1 to 5, respectively.

An algorithm was developed based on the TS825 method and compared with EnergyPlus simulation results that was developed based on heat balance method. The comparison can be done only for heating load due to the insufficiency of the TS825 method for calculating the cooling load. In annual scale, the deviation between calculated heating loads were 39.5 % for Mersin (highest) and 1.9 % for Ankara (lowest). According to heat balance method, cooling loads were determined as 128.2 kWh/m$^2$y for Mersin, 70.7 kWh/m$^2$y for Istanbul, 49.0 kWh/m$^2$y for Erzincan, 44.9 kWh/m$^2$y for Ankara and 26.7 kWh/m$^2$y for Erzurum.

TS825 method calculates heating load under steady-state conditions, heat balance method includes instantaneous meteorological data change in heating-cooling load calculations. Moreover, thermal mass calculations which represent energy storage in building construction elements realize the obtained results. Differences between those two methods show that TS825 method is not sufficient for building efficiency studies. Improvement in TS825 method according to other method leads to accurate system selection. In that way, building energy performance will improve, $CO_2$ emission rate will be decreased.

Finally, attempts to enhance building energy performance and to reduce building energy consumption require accurate methods and logical details. It is obvious that TS825 is not sufficient for building energy efficiency studies. Both using monthly average meteorological data and lack of cooling calculation with HVAC system entry, TS825 standard ignores building energy saving potential.

## REFERENCES

ASHRAE Guideline 14 (2014). *Measurement of energy, demand, and water savings*, American Society of Heating, Ventilating, and Air Conditioning Engineers, Atlanta, GA, USA.

Harish V. S. K. V. and Kumar, A. (2016). "A review on modeling and simulation of building energy systems." *Renewable Sustainable Energy Reviews*, Vol. 56, pp. 1272-92. doi:10.1016/j.rser.2015.12.040.

Keskin, T. (2010). Binalar sektörü mevcut durum değerlendirmesi raporu. http://iklim.cob.gov.tr/iklim/Files/Enerji_Sektoru_Mevcut_Durum_Degerlendirmesi_Raporu.pdf [Accessed 27.05.2017].

Kürekçi A., Bardakçı, A. T., Çubuk, H. and Emanet, Ö. (2012) "Türkiye'nin tüm illeri için optimum yalıtım kalınlığının belirlenmesi." *Tesisat Mühendisliği Dergisi*, Vol. 131, pp. 5-21.

Özkan, D. B., Onan, C. and Erdem, S. (2009). "Effect of insulation material thickness on thermal insulation." *Sigma - Journal of Engineering and Natural Sciences*, Vol. 27, pp. 190-196.

Perez-Lombard, L., Ortiz, J. and Pout, C. (2008). "A review on buildings energy consumption information." *Energy and Buildings*, Vol. 40, No. 3, pp. 394–398.

Stadler, M., Firestone, R., Curtil, D. and Marnay, C. (2006). "On-site generation simulation with EnergyPlus for commercial buildings." *ACEEE Summer Study on Energy Efficiency in Buildings*, pp. 242-254.

The Republic of Turkey, Ministry of Energy and Natural Resources, http://www.eigm.gov.tr/tr-TR/Denge-Tablolari/Denge-Tablolari [Accessed 28.02.2016].

The Republic of Turkey, Ministry of Energy and Natural Resources, http://www.eie.gov.tr/ [Accessed 08.03.2016].

TS EN ISO 14683 (2009). *Thermal bridges in building construction-linear thermal transmittance-simplified method and default values*, Turkish Standard Institution, Ankara, Turkey.

TS 825 (2013). Thermal insulation requirements for buildings, Turkish Standards Institution, Ankara, Turkey.

U.S. Department of Energy, http://www.energy.gov/, Washington, USA, [Accessed 23.05.2017].

Walton G. N. (1983). "Thermal Analysis Research Program Reference Manual". National Bureau of Standards.

# Turkish Journal of Engineering

*Turkish Journal of Engineering (TUJE)*
*Vol. 1, Issue 1, pp. 11-17, May 2017*
*ISSN 2587-1366, Turkey*
*DOI: 10.31127/tuje.315927*
*Research Article*

## TREATMENT OF BIODIESEL WASTEWATER USING YELLOW MUSTARD SEEDS

Serpil Savcı *[1]

[1] Bozok University, Engineering Arthitecture Faculty, Biosystems Engineering Department, Yozgat, Turkey
(serpil.savci@bozok.edu.tr)

* Corresponding Author
Received: 31/03/2017 Accepted: 02/05/2017

**ABSTRACT**
In this study, removal of original biodiesel wastewater (BOD, COD, oil&greas) by yellow mustard seeds was examined by a batch system. The effect of the adsorption time 300 minutes, adsorbent dose (1.0 g/L) and mixing rate (120 rpm) on the adsorption capacity of pollutants. The applicability of the Langmuir and Freundlich isotherms were examined. According to the data obtained from experiments, biodiesel wastewater can be treated by adsorption using yellow mustard seeds.

***Keywords:*** *Biodiesel wastewater, Agricultural waste, Adsorption, Isotherm*

## 1. INTRODUCTION

Fossil fuels are non-renewable and limited sources in the World. For this reason, people search for new, sustainable, alternative, environmentally and renewable power sources. Today, biodiesel has an attracted much more attention for biodegradable, nontoxic, renewable, burns with a low sulfur, carbon monoxide and lower harmful emissions. Biodiesel is produced from the transesterification reaction in the presence of alcohols and catalyst (Ngamlerdpokin *et al*., 2011; Jaruvat *et al*., 2010; Rattanapan *et al*., 2011; Ceclan *et al*., 2012). Washing process is produced biodiesel wastewater. The washing process is remove soap, suspanded solids and residual alcohol (Daut *et al*., 2015; Srirangsan *et al*., 2009). It is depending on the impurity level of methyl ester, with about 20–120 L of wastewater being generated per 100 L biodiesel produced.

There are many physico-chemical proses for removal of polluted from wastewater. However, these methods are too expensive also they are doing secondary pollution. For this reason, both environmental friendly and low-cost effective methods should be investigated. Adsorption is the one of the most promising method for treatment wastewater. The adsorption which is a simple, effective and low-cost process compared to other processes (Elkady *et al*., 2011). Although activated carbon is the best adsorbent in removal of chemical substances from wastewater, there are many negative aspects such as they are expensive and washing needs (McKay, 1981; McKay, 1982; Blum *et al*., 1993; Meshko *et al*., 2001). After that scientist are working adsorbents that they are inexpensive. Peat (Xiong and Mahmood, 2010; Calderón *et al*., 2008); agricultural waste (Mittal *et al*., 2006; Moussavi *et al*., 2010), chitin (Gupta *et al*., 2012; Sokker *et al*., 2011) are low cost adsorbent for using adsorption. Liu et al., (2009) used adsorption processed biodiesel washwaters for the glycerol in conical flasks with continuous shaking. They used activated carbon, clay minerals, natural and synthetic zeolites as an adsorbent. According to the results, activated carbon has the highest adsorption capability of glycerol from aqueous solution. Another study reported by Pitakpoolsil and Hunsom (2014), for biodiesel wastewater and commercial chitosan flakes (Pitakpoolsil *et al*., 2014). According to the study, the biological oxygen demand (BOD), chemical oxygen demand (COD) and oil & grease were removed by batch system. Assawasaengrat et al., (2015) used magnesium silicate as an adsorbent for removal of free fatty acid (FFA), soap and glycerine from biodiesel (Assawasaengrat *et al*., 2015).

When Rudolph Diesel invented diesel engines that they are using agricultural sector, vegetable oils were used for producing biodiesel. The first biofuel patents around the world, Professor Expedito José de Sá Parente, is considered by many to be the inventor of biodiesel. The first small pilot biodiesel plant was built in 1985 in Austria. After that the biodiesel plant that it is working with microalge was built in New Mexico in 1987. Figure 1 shows The world's biggest biodiesel producers in 2015, by country (in billion liters).

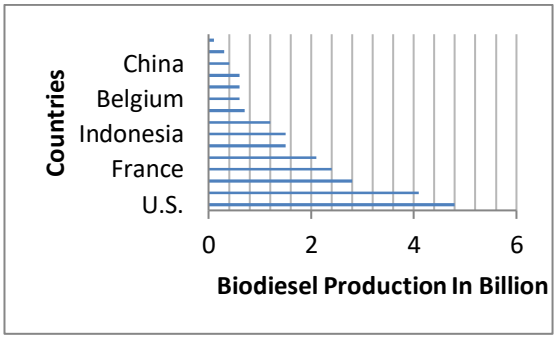


Fig. 1. The world's biggest biodiesel producers in 2015, by country (in billion liters) (The Statistic Portal, 2017).

Actually, main source of biodiesel is plants oil. Plant oil types are depending on climatic factors and soil properties in their countries. Biodiesel producers use palm oil for producing biodiesel in Thailand. In the U.S. they use soybean. In Malaysia, they use palm oil. The palm oil is the most common feed stocks for biodiesel production. Because biodiesel producers get palm oil very easily and palm oil have all-purpose applications. Table 1 depicts the oil sources suitable for biodiesel production.

Table 1. Raw materials for biodiesel production (Olkiewicz *et al*., 2016; Verma and Sharma 2016; Tubino *et al*., 2014; Verma *et al*., 2015).

| Edible | Non-edible | Other |
|---|---|---|
| Soubean oil | Karanja (Pongamia oil) | Waste cooking oil |
| Palm oil | Mahua oil | Microalgae |
| Canola oil | Neem | Fish oil |
| Sunflower oil | *Jatropha curcas* | Beef tallow |
| Cottonseed oil | *Pongamia pinnata (Karanja Yağı)* | Poultry fat |
| Maize oil | Sea mango | Chicken fat |
| Penut oil | Jatropha oil | Chlorella protothecoides microalgae |
| Coconut oil | Linseed | Spirulina platensis algae |
| Mustard oil | Rubber seed | Sewage sludge |

The using of waste cooking oil is one of the basic idea for the produce of biodiesel. The using of waste cooking oil in biodiesel producing is very useful for environment and ecology. Because these oils are prevented from being discharged to the drainage system (Kumar and Sharma 2015; Kwon *et al*., 2012; Zhan *et al*., 2013). Microalgae are the one of the important raw material for biodiesel production due to their fast growth and easy cultivation (Tsigie *et al*., 2012).

In this work was focused on investigating the treatment of biodiesel wastewater by batch system using yellow mustard seeds.

## 2. MATERIAL AND METHODS

### 2.1. Material

#### *2.1.1. Yellow Mustard Seeds*

The seeds of yellow mustard were supplied from Biofuel Laboratory in Yozgat. The crude oil was obtained by screw press. Figure 2 shows that seeds before grinding and after grinding.


Fig. 2. a) seeds before grinding b) after grinding

#### *2.1.2. Wastewater*

Original biodiesel wastewater used in this study. It was collected from Biofuel Laboratory of Department of Biosystems Engineering in Bozok University in Yozgat in Turkey. This Plant uses mustard seeds as a raw material. Biodiesel is washed in transesterification method. Wastewater are obtained by transesterification method. The characteristic of wastewater were analyzed according to the standard methods (Standard Methods, 1998). Biodiesel wastewater before treatment is as presented Fig 3.

Fig. 3. Biodiesel wastewater before treatment

### 2.2. Methods

Biodiesel wastewater was selected as an adsorbate for carrying out the adsorption studies on oil cake was obtained from Bozok University Biosystems Engineering Department Laboratory. Original biodiesel wastewater was obtained from Energy Systems Laboratory in Turkey. Figure 4 presented adsorption of biodiesel wastewater.

Fig. 4. Adsorption of biodiesel wastewater

To estimated that batch experiment was performed using biodiesel wastewater as the adsorbate onto oil cake. Equilibrium tests were done by contacting 1.0 g of waste ash with 1000 mL of biodiesel wastewater at different initials concentrations at room temperature (25 $^{0}$C). The incubation times ranged from 60 to 300 minutes. The wastewater was separated from the supernatant and adsorbate by vacuum filtration through filter paper No:1 (Whatman 70 mm). All experiments were conducted twice.

#### *2.2.1. Calculation*

The amount of original biodiesel wastewater adsorbed by agriculture waste was calculated using the mass balance equation:

$$qt = \frac{(C_0 - Ct)V}{m} \quad (1)$$

and the amount of original biodiesel wastewater removed (%) was calculated above:

$$\text{Removal (\%)} = \frac{C_0 - Ct}{C_0} \times 100\% \quad (2)$$

where qt (mg/g) is the amount of biodiesel wastewater adsorbed by agriculture waste $C_0$ and Ct (mg/L) are the initial original biodiesel wastewater concentration at any time t, V is the volume of the original biodiesel wastewater solution (L); and m is the amount of agriculture waste (g) (Baek *et al.*, 2010).

Langmuir and Freundlich models were employed for adsorption isotherm model. The linearized form of the Langmuir model can be written as (Ho, 2006):

$$\frac{C_e}{q_e} = \frac{1}{K_L} + (\frac{a_L}{K_L})C_e \quad (3)$$

where; Ce = the equilibrium concentration of adsorbate in solution after adsorption (mg/L),
qe = the equilibrium solid phase concentration (mg/g), $K_L$ (L/g) and aL (L/mg) = the Langmuir constants.

The linearized form of the Freundlich model can be written as:

$$\log q_e = \log K_F + \frac{1}{n}\log C_e \quad (4)$$

where;
Ce = the equilibrium concentration of adsorbate in solution after adsorption (mg/L),
qe = the equilibrium solid phase concentration (mg/g),
$K_F$ (L/g) and Freundlich constants (n) related with adsorption capacity and intensity.

## 3. RESULTS AND DISCUSSION

Original biodiesel wastewater used in this study and characteristic of biodiesel wastewater show in Table 1. The effect of the adsorption time 300 minutes, adsorbent dose (1.0 g/L) and mixing rate (120 rpm) on the adsorption capacity of pollutants. The biodiesel wastewater adsorption equilibrium was attained within 180 min.

Pitakpoolsil *et al.* (2013) were also found similar results for biodiesel wastewater and chitosan flakes systems. Initial adsorption tests showed that yellow mustard seeds adsorbed biodiesel wastewater (Fig. 5) (Pitakpoolsil and Hunsom 2013).

Table 2. Biodiesel wastewater characteristic used in the experiment

| Parameter (mg/L) | Test Result |
|---|---|
| Oil&grease | 7457 |
| TDS | 15165 |
| TSS | 1363 |
| COD | 85904 |
| BOD | 25901 |

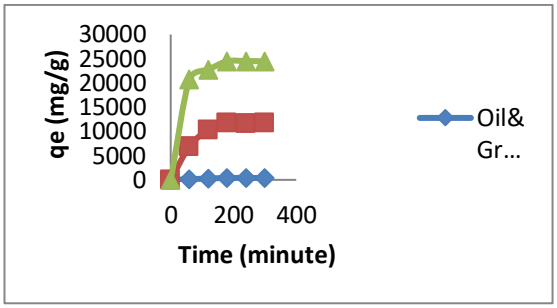


Fig. 5. Effect of the time on the adsorption capacity

Several adsorption isotherms were studied in order to identify the optimization conditions of an adsorption system for removal of BOD, COD, oil&grease from biodiesel wasteater. The adsorption data of the BOD, COD, oil&grease on the yellow mustard seeds were analyzed using Langmuir and Freundlich models.

Figure 6-7-8 show the Langmuir isotherms for oil&grease, BOD, COD whereas the isotherm constants are presented in Table 3-4. As can be seen from Table 2-3, although better correlation coefficient was obtained from Langmuir and Freundlich isotherm model, however values of $q_{max}$ and n were found negative. These negative value was also reported by Robinson *et al*. (2002) and Basibuyuk *et al.*, (2007).

Table 3. Langmuir Isotherm Constants

| Parameters | $q_{max}$ (mg/g) | $a_L$ (L/mg) | $K_L$ (L/g) | $R^2$ |
|---|---|---|---|---|
| BOD | -4.043 | -15281.9019 | 6.1785 | 0.9999 |
| COD | 26.287 | -0.002758 | -0.0725 | 0.9982 |
| Oil-grease | 32.102 | -0.000176 | -0.00565 | 0.9937 |

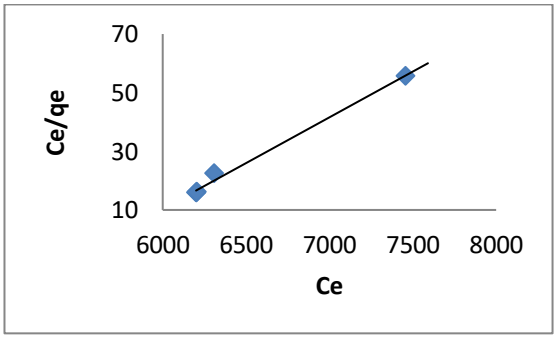


Fig. 6. Langmuir Isotherm for oil&grease

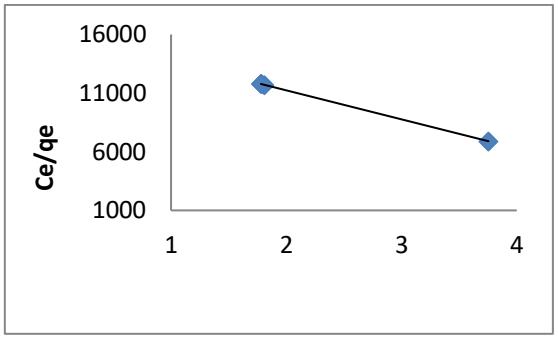


Fig. 7. Langmuir Isotherm For BOD

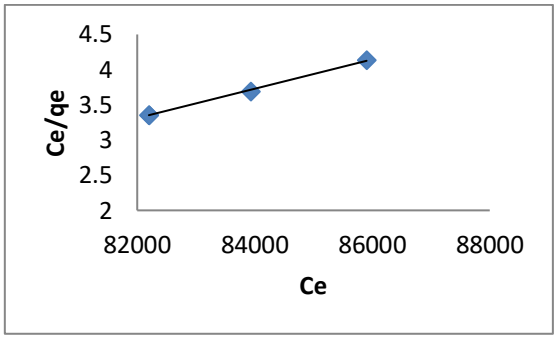


Fig. 8. Langmuir Isotherm For COD

Figure 9-10-11 show the Freundlich isotherms for oil&grease, BOD, COD whereas the isotherm constants are seen in Table 3.

Table 4. Freundlich Isotherm Constants

| Parameters | $K_f$ (L/g) | n | $R^2$ |
|---|---|---|---|
| BOD | 1.452 | -0.389 | 0.9999 |
| COD | 4.064 | -0.269 | 0.9993 |
| Oil&grease | 5.584 | -0.179 | 0.9536 |

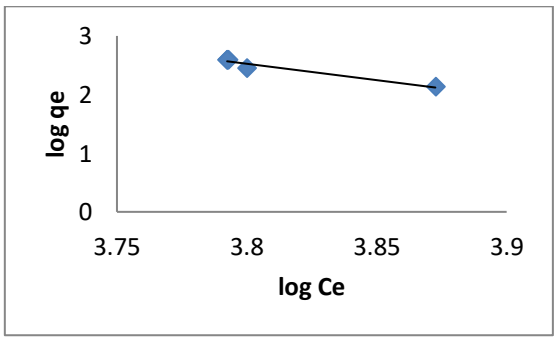


Fig. 9. Freundlich Isotherm For oil&grease

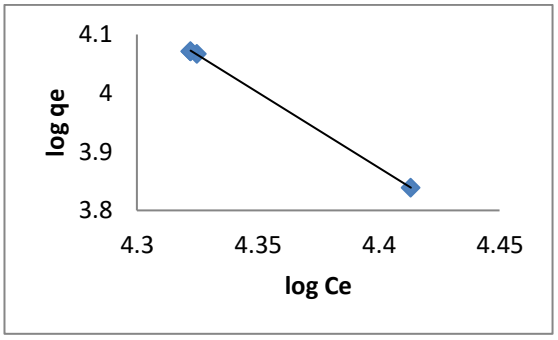


Fig. 10. Freundlich Isotherm For BOD

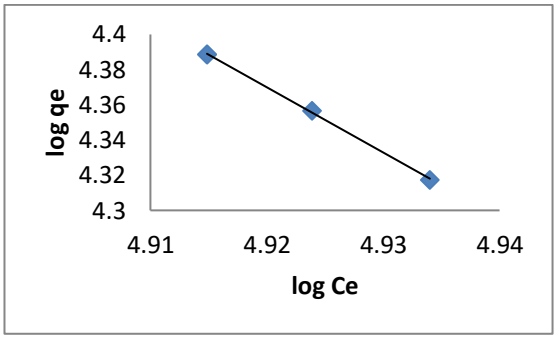


Fig. 11. Freundlich Isotherm For COD

## 4. CONCLUSIONS

This study has shown that adsorption is a useful method as a treatment of polluted from biodiesel wastewater such as COD, BOD, oil&greas. The treatment of biodiesel wastewater was carried out in laboratory conditions (25 $^0$C). The effect of the adsorption time 300 minutes, adsorbent dose (1.0 g/L) and mixing rate (120 rpm) on the adsorption capacity of pollutants. Data obtained from equilibrium studies fit both Langmuir and Freundlich models however for the both Langmuir and Freundlich model negative values were obtained and indicating the inadequacy of these models for these particular wastewater-yellow mustard seeds system.

## ACKNOWLEDGMENTS

The author would like to thank Bozok University BAP (Project No: 2015MMF/A217) for financial support and Mersin University Environmental Engineering Department for laboratory facilities and materials support.

## REFERENCES

Assawasaengrat, P., Jintanavasan, P. and Kitchaiya, P. (2015). Adsorption of FFA, Soap and Glycerine in Biodiesel Using Magnesium Silicate, *Chemical Engineering Transactions*, Vol. 43, No 43, pp. 1135-1140.

Baek, M. H., Ijagbemi, C. O., Se-Jin O amd Kim, D. S. (2010). Removal of Malachite Green from aqueous

solution using degreased coffee bean, *Journal of Hazardous Materials* Vol. 176, pp. 820–828.

Basibuyuk, M., Savcı, S., Keskinkan, O. and Cakmak, M. E. (2007). Investigation of a Basic Dye Adsorption Characteristics of a Non-Living Submerged Aquatic Plant (*Myriophyllum spicatum*), *Asian Journal of Chemistry*, Vol.3, No. 19, pp. 1693-1702.

Blum, D. J. W., Suffet, I. H. and Duguet, J. P. (1993). Estimating The Activated Carbon Adsorption of Organic Chemicals In Water. Crit. Rev. *Environ. Science Technol.*, Vol.23, pp.121-136.

Calderón, M., et al., (2008). The use of Magallanic peat as non-conventional sorbent for EDTA removal from wastewater.*Bioresource Technology* 99.17 8130-8136.

Ceclan R. E., Pop A. and Ceclan M., (2012). Biodiesel from Waste Vegetable Oils, *Chemical Engineering Transactions*, Vol. 29, pp. 1177-1182.

Daud, N. M., Abdullah, S. R. S., Hasan, H. A. and Yaakob, Z. (2015). Production of biodiesel and its wastewater treatment technologies: A review. *Process Safety and Environmental Protection* Vol.9, No. 4, pp.487–508.

Elkady M. F., Ibrahim A.M. and Abd El-Latif M. M. (2011). Assessment of the adsorption kinetics, equilibrium and thermodynamic for the potential removal of reactive red dye using eggshell biocomposite beads. *Desalination*; Vol. 278, No. 1, pp. 412-23.

Gupta, N., Kushwaha, A. K., Chattopadhyaya, M. C., (2012). Adsorptive removal of $Pb^{2+}$, $Co^{2+}$ and $Ni^{2+}$ by hydroxyapatite/chitosan composite from aqueous solution. *Journal of the Taiwan Institute of Chemical Engineers* Vol.43, No.1, pp. 125-131.

Ho YS., (2006). Isotherms for the sorption of lead onto peat: comparison of linear and non-linear methods. *Polish Journal of Environmental Study* Vol. 15, pp. 81–6.

Jaruwat, P., Kongjao, S., & Hunsom, M. (2010). Management of biodiesel wastewater by the combined processes of chemical recovery and electrochemical treatment. *Energy Conversion and Management*, Vol. 51, No.3, pp. 531–537.

Kumar M, Sharma MP., (2016). Kinetics of Chlorella protothecoides microalgal oil using base catalyst. *Egypt Journal of Petrolium*, Vol. 25, No.3, pp. 375-382.

Kwon E.E., Kim S, Jeon Y.J., Yi H., (2012). Biodiesel production from sewage sludge: new paradigm for mining energy from municipal hazardous material. *Environ Sci Technol*; Vol.46, pp.10222–8.

Liu, S., Musuku, S. R., Adhikari, S., Fernando, S., (2009). Adsorption of glycerol from biodiesel washwaters, *Environmental Technology* Vol. 30, No. 5, pp. 505–510.

McKay, G., (1981). Design Models For Adsorption System In Wastewater Treatment. *J. Chem. Tech. Biotechnol.*, Vol.31, pp. 717-772.

McKay, G., (1982). Adsorption of Dyestuffs From Aqueous Solutions With Activated Carbon I: Equilibrium and Batch Contact-Time Studies. *J. Chem. Tech. Biotechnol.*, Vol. 32 pp. 759-731.

Meshko, V., Markovska, L., Mincheva, M., Rodrigues, A.E., (2001). Adsorption of Basic Dyes On Granular Acivated Carbon and Natural Zeolite. *Water Research*, Vol. 35, No.14 pp. 3357-3366.

Ngamlerdpokin, K., Kumjadpai, S., Chatanon, P., Tungmanee, U., Chuenchuanchom, S., Jaruwat, P., Hunsom, M. (2011). Remediation of biodiesel wastewater by chemical- and electro-coagulation: A comparative study. *Journal of Environmental Management*, Vol. 92, No.10, pp. 2454– 2460.

Mittal, Alok, Jyoti Mittal, and Lisha Kurup, (2006). Adsorption isotherms, kinetics and column operations for the removal of hazardous dye, Tartrazine from aqueous solutions using waste materials—bottom ash and de-oiled soya, as adsorbents. *Journal of Hazardous Materials*, Vol. 136, No.3 pp. 567-578.

Moussavi, Gholamreza, and Behnam Barikbin (2010). Biosorption of chromium (VI) from industrial wastewater onto pistachio hull waste biomass. *Chemical Engineering Journal*, Vol.162, No:3, pp. 893-900.

Pitakpoolsil, Wipawan, and Mali Hunsom, (2014). Treatment of biodiesel wastewater by adsorption with commercial chitosan flakes: parameter optimization and process kinetics. *Journal of Environmental Management* Vol.133 pp. 284-292.

Pitakpoolsil, W., Hunsom M., (2013). Adsorption of pollutants from biodiesel wastewater using chitosan flakes. *Journal of the Taiwan Institute of Chemical Engineers* Vol.44, pp.963–971.

Robinson T., Chandran B., Nigam, P., (2002). Removal of dyes from a synthetic textile dye effluent by biosorption on apple pomace and wheat straw, *Water Research.*, Vol. 36, No.11, pp. 2824-2830.

Rattanapan, C., Sawain, A., Suksaroj, T., & Suksaroj, C. (2011). Enhanced efficiency of dissolved air flotation for biodiesel wastewater treatment by acidification and coagulation processes. *Desalination*, Vol. 280, No.1-3, pp. 370–377.

Srirangsan, A., Ongwandee, M., Chavalparit, O., (2009). Treatment of biodiesel wastewater by electrocoagulation process. *Environ. Asia*, Vol.2, pp.15–19.

Standart Methods, A. P. H. A.-A. W. W. A. W. P. C. F., 1998. Standart Methods For The Examination Of Water And Wastewater. 19. Baskı, Washington, D.C.

Sokker, H. H., El-Sawy N. M., Hassan, M. A., El-Anadouli B. E., (2011). Adsorption of crude oil from aqueous solution by hydrogel of chitosan based

polyacrylamide prepared by radiation induced graft polymerization. *Journal of Hazardous Materials* Vol.190, No.1, pp. 359-365.

The Statistic Portal (http://www.statista.com/statistics/271472/biodiesel-production-in-selected-countries/) 02.05.2017.

Tubino M, Junior JGR, Bauerfeldt GF., (2014). Biodiesel synthesis with alkaline catalysts: a new refractometric monitoring and kinetic study. *Fuel*, Vol. 125, pp. 164– 72.

Tsigie, Y. A., Huynh, L. H., Ismadji, S., Engida, A. M., Ju, Y. H., (2012). In situ biodiesel production from wet Chlorella vulgaris under subcritical condition. *Chemical Engineering Journal*, Vol. 213, pp.104–108.

Olkiewicz, M., Torres, C. M., Jiménez, L., Font, J., Bengoa, C., (2016). Scale-up and economic analysis of biodiesel production from municipal primary sewage sludge. *Bioresource Technology*, Vol. 214, pp.122–131.

Verma, P., Sharma, M. P., (2016). Review of process parameters for biodiesel production from different feedstocks, *Renewable and Sustainable Energy Reviews*, Vol. 62, pp.1063–1071.

Verma P, Sharma MP, Dwivedi G., (2015). Operational and environmental impact of biodiesel on engine performance: a review of literature. *Int J Renew Energy Res*;Vol. 5, No:4, pp. 961–70.

Xiong, J.B., Mahmood, Q., (2010). Adsorptive removal of phosphate from aqueous media by peat. *Desalination* 259:59–64.

Zhang X, Yan S, Tyagi R.D, Surampalli R.Y., (2013). Energy balance and greenhouse gas emissions of biodiesel production from oil derived from wastewater and wastewater sludge. *Renew Energy*; Vol. 55, pp.392–403.

# Turkish Journal of Engineering

*Turkish Journal of Engineering (TUJE)*
*Vol. 1, Issue 1, pp. 18-24, May 2017*
*ISSN 2587-1366, Turkey*
*DOI: 10.31127/tuje.316665*
*Research Article*


## EVALUATION OF THE SOIL CHARACTERISTICS AND LIQUEFACTION RISK IN KAZIMPASA, ADAPAZARI (TURKEY), CASE STUDY


T. Fikret Kurnaz *[1]

[1] Mersin University, Technical Sciences Vocational School, Department of Transportation Services, Mersin, Turkey (fkurnaz@mersin.edu.tr)

* Corresponding Author


Received: 02/04/2017 Accepted: 03/05/2017



**ABSTRACT**
It is necessary to determine the local soil properties in order to safe constructions in settlement areas under the earthquake hazard. In this study, the local soil conditions of Kazimpasa region in Adapazari were investigated by geological, geophysical and geotechnical data in order to evaluate the soil characteristics and liquefaction risk. 19 seismic and 19 drilling studies results have been evaluated to determine the soil characteristics of the study area. The study area is located in the 1st degree earthquake zone. The geology of the study area is generally controlled by Quaternary aged alluvium and Eocene aged claystones. The local soil classes were determined as Z4 in the alluvium and Z2 in some areas controlled by altered claystones in the study area. The P-wave velocities were measured between 333 - 2026 m/s and the S-wave velocities were measured between 118 - 1089 m/s according to the seismic studies. The ground water level in the alluvium is varying between 0 – 3 m. The liquefaction analysis results indicated that some areas covered with alluvium have liquefaction potential considering the soil properties and seismic activities of the study area.



***Keywords:*** *Soil investigation, geotechnics, geophysics, liquefaction, Kazimpasa*

## 1. INTRODUCTION

17 August 1999 Kocaeli Earthquake has strongly influenced the eastern parts of the Marmara Region. Adapazari city was heavily damaged due to the close to the epicenter of the earthquake, the building quality and the local soil conditions. It has been revealed many times by various researchers that the damages that occurred during the earthquakes were affected by local ground conditions. During the Kocaeli earthquake of 17 August 1999, a large part of the buildings in Adapazari were exposed to the settle, tilt and collapse due to the local soil conditions. Adapazari city is mostly located on thick alluvial deposits near the North Anatolian Fault (Yılmaz et al. 2004). Therefore, it has a strongly liquefaction potential during major earthquakes. There have been carried out many studies related the local soil conditions of Adapazari city, the effects of geotechnical factors on observed damages, liquefaction, loss of bearing capacity and ground deformations by many researchers (Erken et al. 2003; Kaya et al. 2002; Kiku et al. 2001, Kutanis and Bal, 2006, Yılmaz et al. 2011, Sert et al. 2005, Sancio et al. 2002, Bol et al. 2008, Jonathan et al. 2004).

The thickness of the alluvium layer in the Adapazari region is about 1 km (Komazawa et al. 2002). This thick alluvium layer is formed by Holocene aged sediments carried by Sakarya and Cark rivers. The soft and unconsolidated sediment layers have caused ground deformations during major earthquakes in the region. The most important has been the liquefaction. The liquefaction can be explain as the increase of the pore water pressure, the decrease of the effective stress and the behavior of the ground as a liquid due to the disappearance of the sliding resistance especially as a result of cyclic loads on saturated loose soils. Soil liquefaction causes many damages during the earthquake such as settling and tilting in structures with shallow and deep foundations and outcropping in underground transport lines. In addition, flow-type migrations in slopes and lateral spreading types in flat and less inclined lands can occur as a result of liquefaction. The damages due to liquefaction observed in many regions around the world, have been instrumental in the development of sensitivity of the determination of the risk of liquefaction especially in regions with earthquake hazard. For these reasons, determining the liquefaction sensitivity of the ground during earthquakes is a very important issue in terms of geotechnical engineering.

In this study, the soil characteristics of the Kazimpasa region which is located on the western part of Adapazari city were evaluated (Figure 1). In order to evaluate the soil conditions of the study area, totally 19 drilling, 19 seismic studies data and soil - rock samples laboratory tests results have been used. In addition, liquefaction analyzes based on SPT (Standart Penetration Test) method were performed to determine the liquefaction potential of the study area.

## 2. LIQUEFACTION

The water saturated, loose sand / sandy soils tend to compression and volumetric contraction under the cyclic loads effect. This tendency increases the water pressure in the absence of drainage. When the cyclic loads supports the increase of the water pressure in sand layer the total normal stress can reach equal values with water pressure (Das, 1983). In this case, noncohesive soil loses the shear strength and exposed to large displacement by acting as a liquid. So, the liquefaction phase begins (Das, 1983).

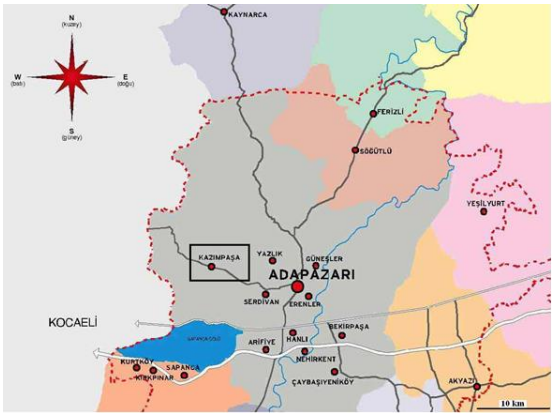


Fig. 1. The location of the study area

Simplified procedure development studies to assess the liquefaction sensitivity of the soils were first performed by Seed and Idriss (1971). This study, which is the basis for liquefaction analysis has updated, improved over time and begun to be discussed in detail especially in the early 2000s (Youd et al. 2001; Cetin et al. 2004; Idriss ve Boulanger, 2008, Idriss ve Boulanger, 2010, Boulanger ve Idriss, 2014). The procedure recommended by especially Youd et al. (2001) is a widely used method to determine the liquefaction sensitivity of soils in Turkey as in many countries of the world. In this method, the safety of the soil against liquefaction during an earthquake expressed in the form of comparison of the rate of cyclic resistance of the soil with the rate of cyclic stresses due to earthquakes. The ratio of cyclic stress generated during earthquakes ($CSR$) is defined by Seed and Idriss (1971) as in Equation 1.

$$CSR = 0.65 \times \frac{a_{max}}{g} \times \frac{\sigma_v}{\sigma_v'} \times r_d \qquad (1)$$

Here is, $a_{max}$, the peak horizontal acceleration at the ground surface during the earthquake; $g$, gravitational acceleration; $\sigma_v$ and $\sigma_v'$, total and effective stress; $r_d$, stress reduction coefficient. The average values are used for the $r_d$ depending on the depth in the Equation 2 in engineering applications.

$$r_d = \begin{cases} 1.0 - 0.00765z, & z \leq 9.15 \text{ m} \\ 1.174 - 0.0267z, & 9.15 < z \leq 23 \text{ m} \end{cases} \qquad (2)$$

The most plausible way to determine the rate of cyclic resistance of soils is to conduct laboratory tests on undisturbed samples taken from the field. However, due to the disturbeds, during the sampling and factors such as cost the cyclic rate of resistance ($CRR$) is attempted to be estimated based on the standard penetration test (SPT), cone penetration test (CPT) and shear wave velocity (Vs) measurements for constructions except in very special engineering structures. It is seen that liquefaction analysis based on SPT is more preferred method in Turkey.

For sands with a fine grain content, FC ≤ 5% and for Mw = 7.5 magnitude earthquakes, the curve that separates the regions where the liquefaction occurs and is not observed is defined as a clean sand curve by Youd et al. (2001) and the cyclic rate of resistance ($CRR_{7.5}$) is expressed for this situation (Figure 2). The safety factor (FS) against the liquefaction is calculated from Equation 3. The safety factor below 1.0 indicates the presence of liquefaction sensitivity on the soil.

$$FS = \frac{CRR}{CSR} \tag{3}$$

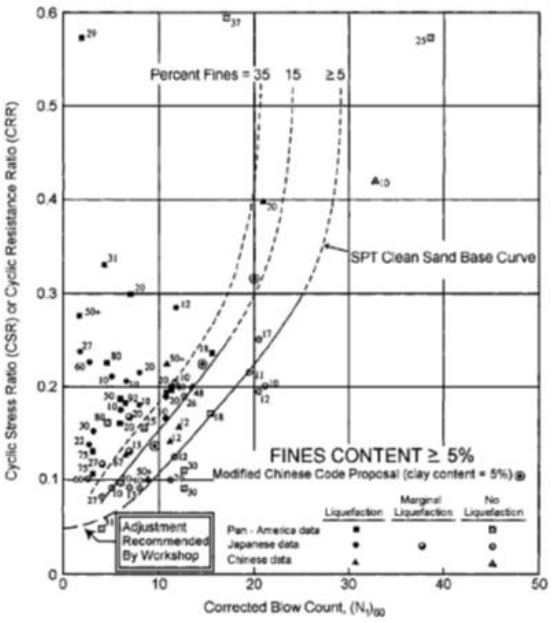


Fig. 2. SPT Clean-Sand Base Curve and Curves for Fines Content = 15% and 35% for Magnitude 7.5 Earthquakes with Data from Liquefaction Case Histories (from Youd et al. 2001)

## 3. GEOLOGICAL SETTINGS AND SEISMICITY

Geological settings in Adapazari plain and its surroundings suggest that downtown Adapazari is developed by fluvial sediments during the past thousands of years. The Sakarya River is a main river in this area runs in the east of the downtown area to Black Sea flowing from south to north. The Cark River one of the rivers branches of the Sakarya River runs to the north passing the south west of the downtown. A large part of the Adapazari plain is consist of deposits of Quaternary aged alluvium containing gravelly and silty sand brought by the rivers (Figure 3). Generally, silt and clay series exist on the ground and gravel, sand, silt series continuously follow the surface series. Dominant ground consists of gravelly and silty sand having different densities and contains low plasticity silty and clay bandage at some places (Onalp et al. 2000). The depth of the bedrock is approximately 1100 m in the center of the city (Komazawa et al. 2002; Hitoshi et al. 2002). The groundwater level is usually 1 to 2 m below the surface of the ground and shows seasonal variations. The ground stratum is usually randomly formed. The thickness of many layers is rarely several meters. Top 5 meters is dominated by silty units. Clays and sands are seen in the form of band. High-plastic clays are seen in old marsh or shallow lakes while sands and silty sands are seen in the old stream beds.

The geology of Kazimpasa region is generally controlled by Quaternary aged alluvium and Eocene aged claystones. The alluvium units are consist of silt, clay, gravel, sand bands, organic matter-rich mud, lake shaft and mud.

The seismotectonic structure threatening Adapazari and its vicinity is the North Anatolian Fault system. The North Anatolian Fault (NAF) which is a right lateral strike fault with a length of 1200 km is located approximately 8 km south of the Adapazari basin. Adapazari has been exposed to several major earthquakes over the last 100 years. In 1943, 1967 and 1999 are the most catastrophic ones occured in the region. The earthquake of Marmara on August 17th 1999 was the most destructive one. Its magnitude was 7.4 (Mw) and associated with faulting over length of 100 -120 km. It was resulted in 17.479 death and 43.953 injured. The government data indicated that %27 of the buildings were either damaged or destroyed, %20 of buildings medium damaged and %53 of building less damaged or undamaged.

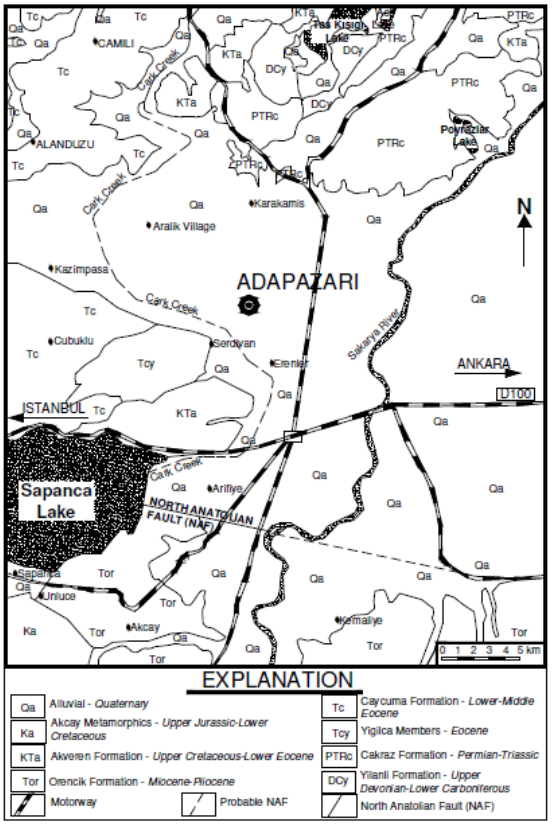


Fig. 3. The geology map of the region.

## 4. GEOPHYSICAL CHARACTERISTICS OF THE STUDY AREA

The geophysical properties of the soils in the study area were evaluated by using 19 seismic fracture measurements. The layer thicknesses, underground velocity structure, dynamic-elastic engineering parameters of the soils were determined depending on

these measurements. The geophone ranges were changed between 2 - 5 m in straight and reverse shots. The device used for seismic refraction application is 12 channels and has a high-mid-low pass filter with a sampling interval of 0.5 ms. Seismic profile lines were chosen to match soil drillings and to best represent the study area. The P-wave velocities were measured between 333 - 2026 m/s and the S-wave velocities were measured between 118 - 1089 m/s in the seismic studies. It was understood that the ground was divided into two or three layers in the study area according to the seismic velocities. The dynamic characteristics of the soils obtained from seismic refraction results are given in Table 1.

## 5. GEOTECHNICAL CHARACTERISTICS OF THE STUDY AREA

In order to determine the geotechnical characteristics of the study area, 19 drilling study results and laboratory samples test results obtained from these drillings have been used. The units cut in drilling wells whose depths are changing between 5 and 15 m are generally alluvium materials and Eocene aged claystones. The drilling locations and distributions were identified considering the geology of the area, covered sections according to field observations. The SPT blow count values determined during the drillings are less than 10 in the near surface alluvium units and changed between 5 and 65 in the study area.

### 5.1. Laboratory Results

The grain size distributions of soils, water content, natural unit weight, atterberg limits and strength properties were determined with laboratory experiments on the 109 disturbed and 17 undisturbed samples taken from the drilling. The laboratory test results related to the disturbed samples are given in Table 2. Sieve analysis and atterberg limits test results were used to classify the soil samples for 109 samples according to the USCS. The soil classes were determined as 75.222% ML, 10.10% SM, 8.26% CL, 5.50% SC and 0.92% GM in the study area. The strength parameters of the alluvial soils in the study area were determined with triaxial compression tests and the results are given in in Table 3

In addition, the soils in the study area were classified according to the regulation on buildings to be made in disaster areas, which was issued in 1998 by the General Directorate of Disaster Affairs. The local soil classes were determined as Z4 in the alluvium and determined as Z2 in altered Eocene aged units.

The superficial appearance of the Eocene aged claystones in the study area is yellow-green brown colored and thin-medium layered. The RQD values are ranged from 0 to 52 and the rock qualities are defined as very poor - poor. The results of uniaxial compression tests on samples of claystones are given in Table 4. The strength values are range from 117.65 to 148.50 kg/cm$^2$ (ASTM 2008) and these are defined as very low strength according to Deere and Miller, (1966).

Table 2. Descriptive statistics of parameters

| | Least | Most | Mean |
|---|---|---|---|
| Gravel % | 12.39 | 44.36 | 21.42 |
| Sand % | 17.56 | 56.78 | 29.64 |
| Clay-Silt % | 19.82 | 70.36 | 48.94 |
| LL % | NP | 42 | 24.36 |
| PL % | NP | 30 | 16.56 |
| PI % | NP | 18 | 8.78 |
| Wn % | 19.32 | 42.36 | 23.48 |
| $\gamma_n$ (gr/cm$^3$) | 1.72 | 20.42 | 1.86 |

Table 3. Triaxial Compression Tests results of the undisturbed samples

| Drilling Number | Depth (m) | c (kPa) | ($\Phi^0$) |
|---|---|---|---|
| D-1 | 2.50 | 74.85 | 7.85 |
| D-2 | 2.50 | 77.08 | 8.04 |
| D-3 | 2.50 | 44.64 | 12.77 |
| D-4 | 2.50 | 82.20 | 7.69 |
| D-5 | 2.50 | 72.26 | 8.36 |
| D-6 | 2.50 | 94.41 | 8.03 |
| D-7 | 2.50 | 82.59 | 7.13 |
| D-9 | 2.50 | 51.81 | 8.84 |
| D-10 | 2.50 | 65.53 | 8.05 |
| D-11 | 2.50 | 75.75 | 7.12 |
| D-12 | 2.50 | 65.53 | 8.05 |
| D-14 | 2.50 | 75.31 | 7.12 |
| D-15 | 2.50 | 70.10 | 7.50 |
| D-16 | 2.50 | 55.76 | 8.14 |
| D-17 | 2.50 | 45.80 | 7.12 |
| D-18 | 2.50 | 74.32 | 7.79 |
| D-19 | 2.50 | 83.53 | 6.12 |

Table 4. Uniaxial Compression Tests results of the claystones

| Drilling Number | Depth (m) | $\sigma_c$ (kg/cm$^2$) |
|---|---|---|
| D-2 | 7.5 | 120.35 |
| D-4 | 3.0 | 138.20 |
| D-5 | 4.5 | 117.65 |
| D-6 | 6.5 | 145.45 |
| D-9 | 6.3 | 115.20 |
| D-11 | 7.4 | 127.80 |
| D-14 | 8.9 | 119.70 |
| D-16 | 4.7 | 148.50 |
| D-17 | 7.5 | 114.84 |

Table 1. Dynamic Elastic Properties Obtained from Seismic Measurements

| Profile No / Layer No | Vp (m/sn) | Vs (m/s) | V. Period sn | Thickness (m) | B. Module ($kg/cm^2$) | Density ($gr/cm^3$) | E. Module ($kg/cm^2$) | Poisson Ratio | S. Module ($kg/cm^2$) |
|---|---|---|---|---|---|---|---|---|---|
| S-1/T1 | 387 | 140 | 0,45 | 3,90 | 1699 | 1.37 | 767 | 0,42 | 269 |
| S-1/T2 | 1152 | 548 | " | | 16736 | 1,81 | 14684 | 0,35 | 5423 |
| S-2/T1 | 392 | 136 | 0,65 | 6,85 | 1779 | 1,38 | 730 | 0,43 | 255 |
| S-2/T2 | 847 | 385 | " | 10,17 | 8692 | 1,67 | 6791 | 0,37 | 2478 |
| S-2/T3 | 1778 | 883 | " | | 42709 | 2,01 | 41947 | 0,33 | 15695 |
| S-3/T1 | 411 | 174 | 0,40 | 3,04 | 1794 | 1,40 | 1175 | 0,39 | 422 |
| S-3/T2 | 1278 | 569 | " | 9,69 | 22271 | 1,85 | 16519 | 0,37 | 6000 |
| S-3/T3 | 1865 | 923 | " | | 47717 | 2,04 | 46436 | 0,33 | 17355 |
| S-4/T1 | 402 | 167 | 0,51 | 2,67 | 1727 | 1,39 | 1080 | 0,39 | 387 |
| S-4/T2 | 939 | 428 | " | 5,62 | 10939 | 1,72 | 8606 | 0,36 | 3143 |
| S-4/T3 | 1625 | 784 | " | | 35843 | 1,97 | 32623 | 0,34 | 12097 |
| S-5/T1 | 365 | 120 | 0,50 | 2,36 | 1545 | 1,35 | 561 | 0,43 | 195 |
| S-5/T2 | 987 | 451 | " | 7,59 | 12214 | 1,74 | 9670 | 0,36 | 3534 |
| S-5/T3 | 1488 | 744 | " | | 28420 | 1,93 | 28420 | 0,33 | 10657 |
| S-6/T1 | 362 | 120 | 0,43 | 2,28 | 1512 | 1,35 | 560 | 0,43 | 194 |
| S-6/T2 | 1179 | 540 | | | 18187 | 1,82 | 14484 | 0,36 | 5296 |
| S-7/T1 | 358 | 120 | 0,68 | 3,02 | 1469 | 1,35 | 557 | 0,43 | 194 |
| S-7/T2 | 785 | 322 | " | 8,05 | 7843 | 1,64 | 4759 | 0,39 | 1701 |
| S-7/T3 | 1420 | 748 | " | | 24175 | 1,90 | 27852 | 0,30 | 10647 |
| S-8/T1 | 339 | 118 | 0,64 | 1,92 | 1281 | 1,33 | 530 | 0,43 | 185 |
| S-8/T2 | 721 | 334 | " | 5,56 | 5961 | 1,61 | 4886 | 0,36 | 1792 |
| S-9/T1 | 388 | 132 | 0,60 | 3,24 | 1751 | 1,38 | 687 | 0,43 | 239 |
| S-9/T2 | 712 | 320 | " | 9,86 | 5931 | 1,60 | 4504 | 0,37 | 1639 |
| S-9/T3 | 1652 | 885 | " | | 33297 | 1,98 | 40207 | 0,29 | 15479 |
| S-10/T1 | 333 | 124 | 0.57 | 1,98 | 1196 | 1,32 | 578 | 0,42 | 203 |
| S-10/T2 | 880 | 380 | " | 6,19 | 9824 | 1,69 | 6755 | 0,38 | 2438 |
| S-11/T1 | 421 | 176 | 0,30 | 2,38 | 1908 | 1,40 | 1212 | 0,39 | 434 |
| S-11/T2 | 1788 | 898 | " | | 42770 | 2,02 | 43283 | 0,33 | 16255 |
| S-12/T1 | 389 | 140 | 0,32 | 2,40 | 1723 | 1,38 | 769 | 0,42 | 269 |
| S-12/T2 | 1659 | 769 | " | | 38852 | 1,98 | 31897 | 0,36 | 11699 |
| S-13/T1 | 413 | 156 | 0,37 | 2,60 | 1930 | 1,40 | 963 | 0,41 | 340 |
| S-13/T2 | 1374 | 622 | " | | 25895 | 1,89 | 20023 | 0,37 | 7301 |
| S-14/T1 | 380 | 140 | 0.48 | 3,07 | 1618 | 1,67 | 762 | 0,42 | 268 |
| S-14/T2 | 1020 | 480 | " | 8,88 | 12845 | 1,75 | 10961 | 0,35 | 4036 |
| S-15/T1 | 425 | 175 | 0,35 | 2,69 | 1967 | 1,41 | 1205 | 0,39 | 431 |
| S-15/T2 | 1335 | 658 | " | 8,57 | 22578 | 1,87 | 21735 | 0,34 | 8113 |
| S-16/T1 | 359 | 130 | 0,4 | 2,60 | 1435 | 1,35 | 649 | 0,42 | 228 |
| S-16/T2 | 1426 | 623 | " | | 28879 | 1,90 | 20437 | 0,38 | 7393 |
| S-17/T1 | 378 | 160 | 0,51 | 2,50 | 1486 | 1,37 | 973 | 0,39 | 349 |
| S-17/T2 | 898 | 420 | " | 8,25 | 9693 | 1,70 | 8142 | 0,36 | 2993 |
| S-17/T3 | 1485 | 770 | " | | 27224 | 1,92 | 30033 | 0,31 | 11409 |
| S-18/T1 | 354 | 133 | 0,56 | 2,14 | 1367 | 1,34 | 674 | 0,41 | 237 |
| S-18/T2 | 862 | 384 | " | 7,06 | 9178 | 1,68 | 6817 | 0,37 | 2476 |
| S-19/T1 | 364 | 124 | 0,56 | 4,11 | 1516 | 1,35 | 597 | 0,43 | 208 |
| S-19/T2 | 781 | 340 | " | 12,19 | 7470 | 1,64 | 5240 | 0,38 | 1894 |

### 5.2. Liquefaction Evaluation of the Study Area

In this study, liquefaction analyzes have been performed for sandy soils based on the procedure recommended by Youd et al. (2001). Different blow counts measured in the field (SPT-N) during the standard penetration tests, fine grain ratios (FC) and depths of groundwater level (hw) as summarized in Chapter 2 were used in the analyzes. In this context, the analyzes were carried out for Mw = 7.5 magnitude earthquake and $a_{max}$ = 0.4g (1st degree earthquake zone) peak ground acceleration and the safety factors (FS) were calculated. It was paid attention the location, soil class and SPT blow count of the soil samples during the decision making of the depths to be analyzed. The analyzes were made for the first 10 m depth and the SPT blow counts for points not exceeding 30 as possible. It has already known that if the safety factor is below 1, it indicates a risk of liquefaction. Situations where the safety factor is between 1 and 1.2 were considered as low risk or possible liquefaction for the study area. A liquefaction hazard map was created for the study area by using the analysis results (Figure 4). There are some local areas especially in the eastern parts of the study area have liquefaction risk as seen in the hazard map.

## 6. CONCLUSIONS

In this study, the geological, geophysical and geotechnical data were used together to determine the soil characteristics and liquefaction potential of Kazimpasa region in Adapazari city. According to the findings obtained, two different geological units are observed in the study area. These are the Quaternary aged alluvium and Eocene aged claytones. Seismic velocities and the SPT blow counts were identified to be low especially in the depths close to the surface in most of the study area. The strength of the Eocene aged claystones was determined as very low seen in some local sides. The liquefaction analyzes showed that some local areas are at risk of liquefaction considering the earthquake hazard and the soft soil characteristics of the study area. It should be useful to take the necessary soil improvement precautions for new constructions to be built in areas of risk of liquefaction in the region.

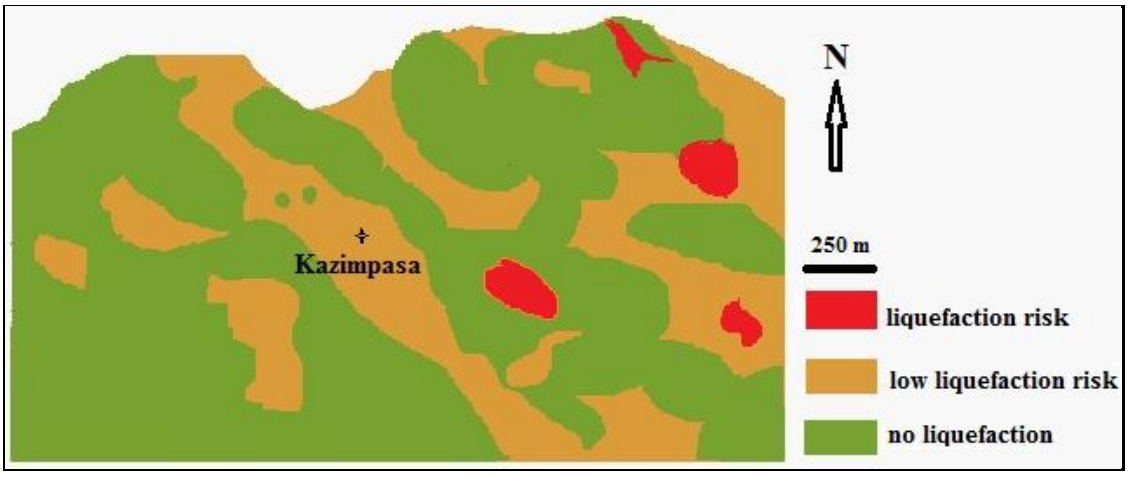


Fig. 4. The liquefaction hazard map of the study area

## REFERENCES

ASTM D4543-08. (2008). Standard Practices for Preparing Rock Core as Cylindrical Test Specimens and verifying Conformance to Dimensional and Shape Tolerances.

Bol, E., Onalp, A., Ozocak, A., (2008). Liquefiability of Silts And The Vulnerability Map of Adapazari. The 14 th World Conference on Earthquake Engineering, Beijing, China.

Boulanger, R. W. & Idriss, I. M. (2014). CPT and SPT based liquefaction triggering procedures. *Report No. UCD/CGM-14/01*, University of California at Davis, 134 pp.

Bray, J.D., Sancio, R.B., Durgunoğlu, H.T., Önalp, A., Youd, T.L., Stewart, J.P., Seed, R.B., Cetin, O.K., Bol, E., Baturay, M.B., Christensen, C., and Karadayılar, T. (2004). Subsurface characterization at ground failure sites in Adapazari, Turkey, J. Geotech. & Geoenv. Engrg., ASCE, 130 (7), 673-685.

Cetin, K. O., Seed, R. B., Der Kiureghian, A., Tokimatsu, K., Harder, L. F., Kayen, R. E., & Moss, R. E. S. (2004). Standard penetration test-based probabilistic and deterministic assessment of seismic soil liquefaction potential. J. Geotech. Geoenviron. Eng., 130(12), 1314-1340.

Das, B.M., (1983). Fundamentals of soil dynamics, Elsevier Science Publishing Co. Inc., s 353-374, New York, USA.

Deere D.V., Miller R.L., 1966, Engineering Classification and Index Properties of Intact Rock, Department of Civil Engineering, University of Illinois, Urbana. pp. 90-101.

Erken, A., Okan, R. ve Erdem, A., (2003). The ground behavior of Adapazarı in 17 August 1999 Kocaeli earthquake., V. National Earthquake Conference, Istanbul, in Turkish.

GDDA (1996). General Directorate of Disaster Affairs, Regulation on buildings to be made in disaster areas. in Turkish.

Hitoshi, M., Jumpei, A., Masao, K., Kajuro, N., Keiichi, N. ve Sumi, S., (2002). Bedrock structure in Adapazarı, Turkey, inferred from gravity anomary and microseisms, Proceedings of the 11th Japan Earthquake Engineering Symposium, 301-306.

Idriss, I. M., & Boulanger, R. W. (2008). Soil liquefaction during earthquakes. EERI Publication, Oakland: CA, 235 pp.

Idriss, I. M., & Boulanger, R. W. (2010). SPT-based liquefaction triggering procedures. Report No. UCD/CGM- 10/02, University of California at Davis, 259 pp.

Kaya, Z., Irisawa, T. ve Erken, A., (2002). Dynamic behavior of Adapazarı soils, 9th National Congress of Soil Mechanics and Foundation Engineering, 220-227, Eskişehir, in Turkish.

Kiku, H., Yoshida, N., Yasuda, S., Irisawa, T., Nakazawa, H., Shimuzu, Y., Ansal, A. ve Erken, A. (2001). In-situ penetrating test and soil profiling in Adapazari-Turkey, XV ICSMGE Satellite Conference on "Lessons Learned from Recent Strong Earthquakes, 259-265, Istanbul, Turkey.

# Turkish Journal of Engineering

*Turkish Journal of Engineering (TUJE)*
*Vol. 1, Issue 1, pp. 25-31, May 2017*
*ISSN 2587-1366, Turkey*
*DOI: 10.31127/tuje.316860*
*Research Article*

## THE OPTIMIZATION OF SURFACE ROUGHNESS OF AZ91D MAGNESIUM ALLOY USING ANOVA IN BALL BURNISHING PROCESS

Berat Barış Buldum *[1] and Süleyman Çınar Çağan [2]

[1] Mersin University, Engineering Faculty, Department of Mechanical Engineering, Mersin, Turkey
(barisbuldum@mersin.edu.tr)

[2] Mersin University, Engineering Faculty, Department of Mechanical Engineering, Mersin, Turkey
(cinarcagan@mersin.edu.tr)

* Corresponding Author
Received: 06/04/2017 Accepted: 05/05/2017

**ABSTRACT**
Ball burnishing is a simple, cost-effective and fast finishing process generally applied to better the surface roughness of machine parts. In this study, the Taguchi $L_{18}$ orthogonal array method is used to find the optimal surface roughness in ball burnishing of AZ91D magnesium alloy. The orthogonal array, the signal-to-noise ratio, and ANOVA (analysis of variance) method is employed to study the performance characteristics in ball burnishing process of AZ91D alloy bars. The purpose of this study is to perform an ANOVA to determine the effects of the (burnishing force, burnishing speed, feed rate and number of passes parameters) on the surface roughness data obtained after the ball burnishing applied to the AZ91D bars. The optimum burnishing parameter was determined based on signal-to-noise (S/N) ratio. Data was analyzed by means of the ANOVA method. The main results of the statistical analysis highlight the great influence of the feed rate, burnishing force and number of passes on surface roughness among the set of factors and their interactions considered.

***Keywords:*** *Surface roughness, Taguchi method, Ball burnishing, ANOVA*

## 1. INTRODUCTION

Magnesium and magnesium alloys have been extensively studied and applied in the automotive, aerospace and defense industries due to their low densities, high strength to weight ratio, high specific toughness and good workability [Buldum et al., 2013, Gnedenkov et al., 2013, Buldum, 2013].

The use of magnesium metal, which has been highly demanded in recent years, is evolving along with industrial and technological developments. Because of the lightness, durability and longevity of magnesium, its use in industry is of interest. [Buldum et al., 2013]. However, due to the disadvantages of cast magnesium alloys such as limited ductility and low fatigue performance, it is difficult to use these materials in load bearing parts of the industry. [Zhang et al., 2005]. But also its use due to its high corrosion sensitivity which is another disadvantage. [Mahajan et al. 2013].

Surface properties of materials are one of the most important parameters in the manufacturing industry. Surface roughness properties are a feature that affects machine performance increase and production costs [Luca et al., 2005]. Machine parts must be manufactured to account for superior dimensional, geometric accuracy and surface roughness to ensure reliable performance and continuous production [Mahajan et al. 2013, Hamamci et al., 2014]. The surface roughness has a significant role in affecting functional characteristics such as corrosion behavior, fatigue strength, wear resistance and power loss because of friction [Mahajan et al. 2013, Hamamci et al., 2014].]. Different methods are used in cases where desired surface roughness values, lathe, milling and conventional grinding cannot be achieved by conventional machining methods.

Burnishing operations are increasingly being demanded as a finishing procedure due to the advantages such as increased surface hardness, fatigue strength and increased wear resistance [López de Lacalle et al., 2005]. Burnishing is generally used to provide good surface roughness. Moreover, these features are provided by inexpensive equipment or fast processing. Ball burnishing is a rapid, simple, practical and affordable mechanical surface treatment (Fig. 1.) [López de Lacalle et al., 2005, Esme, 2010]. Thus, ball burnishing can replace other surface finishing processes, such as lapping, honing, grinding or polishing [Rodriguez et al., 2010].

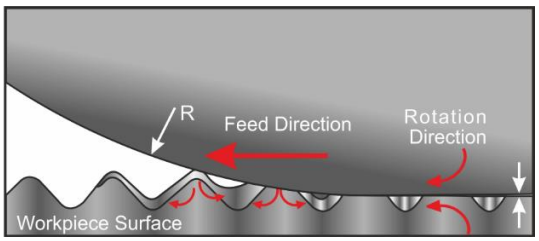


Fig 1. Scheme of Ball burnishing process

The parameters influencing the surface roughness are burnishing speed and force, a number of passes, feed rate, ball material, workpiece material, ball size and lubricant. Many researchers have experimentally explored this process, addressing the effects of burnishing speed and force, feed rate and a number of passes [El-Taweel et al., 2009, Sagbas, 2011, Dabeer et al., 2010, Ibrahim et al., 2009, Low et al., 2011].

In spite of performing ball burnishing process for surface quality development experiments of steel, aluminum, polymer, titanium or nickel made workpiece [López de Lacalle et al., 2005, Sagbas, 2011, Dabeer et al., 2010, Ibrahim et al., 2009, Low et al., 2011, El-Axir et al., 2008, Gokce et al., 2015, Kayali et al., 2013, Grzesik et al., 2012, Thamizhmnaii et al., 2008, Tian et al., 2007], usage of magnesium made workpiece are limited. Work on the development of the above mentioned materials is still being carried out by other researchers in this area.

In the present study, optimization is performed by using the results obtained from our experimental results using the Taguchi method. We used ANOVA method in this analysis. In this view, it is analyzed which parameters used during the experiment are more effective on the surface roughness results and which parameter combinations are efficient. The best burnishing parameters of ball burnishing process of AZ91D magnesium alloy, such as burnishing speed, burnishing force, feed rate, and number of passes of workpiece were found out in order to get the better surface roughness.

## 2. EXPERIMENTAL

Taguchi method has been used widely in engineering analysis to significantly decrease the number experiments [Cicek et al., 2015]. Taguchi method is an important method for the design of high-quality systems and low-cost design solution. Taguchi method exhibits a systematic method that is simple and effective in order to optimize designs for cost, performance and quality [Cicek et al., 2015, Oktem et al., 2006, Pishbin et al., 2010]. Selection of orthogonal array is one of the important steps in Taguchi method. It will further assist to perform experiments to determine the optimum level for each process parameters.

The initial step of Taguchi method is the choice of a proper orthogonal array. The choice of a proper orthogonal array according to the total degrees of freedom of process parameters. In order to choose orthogonal array for experiments properly, the total degrees of freedom needs to be calculated. In this study, three three-levels (Burnishing Force, Burnishing Speed, Feed rate) and one two-levels (Number of passes) as four control factors of mixed level (2 and 3 levels). Therefore, the total degrees of freedom of parameters are equal to 11. Fundamentally, the degrees of freedom for the orthogonal array should be greater than or at least equal to those for the process parameters. Thus, in this study experiments were carried out as per Taguchi's $L_{18}$ ($2^2x3^3$) mixed orthogonal array (Table 1) to optimize of ball burnishing with multiple performance characteristics of the results of surface roughness and microhardness.

Ball burnishing parameters and their limits used in this study are shown in Table 2. The process parameters were determined using MINITAB 17 statistical software based on Taguchi $L_{18}$ orthogonal array.

Table 1. Factors and levels used in the experiment

| Experiment Number | Control factors and levels | | | |
|---|---|---|---|---|
| | Number of passes (A) | Burnishing Force (B) | Burnishing Speed (C) | Feed rate (D) |
| 1 | 1 | 1 | 1 | 1 |
| 2 | 1 | 1 | 2 | 2 |
| 3 | 1 | 1 | 3 | 3 |
| 4 | 1 | 2 | 1 | 1 |
| 5 | 1 | 2 | 2 | 2 |
| 6 | 1 | 2 | 3 | 3 |
| 7 | 1 | 3 | 1 | 2 |
| 8 | 1 | 3 | 2 | 3 |
| 9 | 1 | 3 | 3 | 1 |
| 10 | 2 | 1 | 1 | 3 |
| 11 | 2 | 1 | 2 | 1 |
| 12 | 2 | 1 | 3 | 2 |
| 13 | 2 | 2 | 1 | 2 |
| 14 | 2 | 2 | 2 | 3 |
| 15 | 2 | 2 | 3 | 1 |
| 16 | 2 | 3 | 1 | 3 |
| 17 | 2 | 3 | 2 | 1 |
| 18 | 2 | 3 | 3 | 2 |

Table 2. Process parameters and their limits

| | Factors | Level | | |
|---|---|---|---|---|
| | | 1 | 2 | 3 |
| A | Number of passes | 1 | 2 | - |
| B | Burnishing Force (N) | 50 | 150 | 250 |
| C | Burnishing Speed (rpm) | 200 | 400 | 600 |
| D | Feed rate (mm/min) | 0.1 | 0.25 | 0.5 |

In this study, the experimental material was AZ91D magnesium alloy bar (Yuanhong Alloy Materials Co.,Ltd, China), the chemical composition of which is given in Table 3. This material is widely used in automotive, aerospace and defense industries.

In this work, two specimens were used for AZ91D which the dimension of workpiece material has a diameter of 35 mm and 200 mm in length as demonstrated Fig. 2a. Each specimen was divided into 9 different segments a length of 25 mm and the 5 mm groove between parts. By performing different parameters on each segment.

Table 3. Chemical composition of AZ91D magnesium alloy (wt. %)

| Material | Al | Zn | Mn | Fe | Be | Si | Cu | Ni | Mg |
|---|---|---|---|---|---|---|---|---|---|
| AZ91D | 9.21 | 0.45 | 0.17 | 0.0018 | 0.00084 | 0.016 | 0.002 | 0.00085 | Balance |

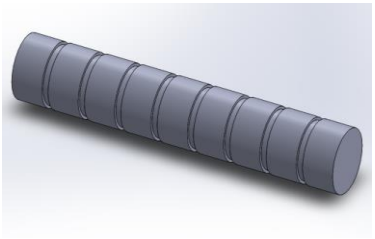

(a)

(b)

Fig 2. a) AZ91D workpiece material, b) CNC lathe

The ball burnishing process was carried out on a CNC lathe as demonstrated Fig. 2b. The experimental set up used for the burnishing experiments is shown in Fig. 3. Also, the force gauge, as shown in Fig. 4., was used to investigate the effect of burnishing force on ball burnishing process. To prevent any particles from ingress the surface of contact between the tool and specimen, cleaning of the ball was carried out during the ball burnishing process. The workpiece was interlocked by the three jaw chuck and tailstock center of the machine. No coolant was used throughout this ball burnishing process.

Fig. 3. The experimental set up

Fig. 4. Force gauge

Average surface roughness values were taken on three different sections of the cylindrical surface along the workpiece (AZ91D magnesium alloy bar). Surface roughness values were measured using a Mitutoyo portable roughness meter model Surftest SJ 201.

ANOVA is basically used in this experiment to determine, which cutting factors mostly affect the roughness value. Basically ANOVA is a collection of statistical models which is used to analyze the variation among the groups. ANOVA is a statistical analysis which is commonly applied to evaluate the data of experiments. In this research, the analysis of direct and interactive effect of the input factors (Burnishing speed, burnishing force, feed rate and number of passes) on the surface roughness is conducted through ANOVA. The regression equation and investigated factors are called to be statistically significant if the p-value in ANOVA result is less than 0.05. Besides, the percentage contribution of terms in the estimated model on the total variation is also considered to evaluate the influence degree of the controllable factors on the model.

## 3. RESULTS AND DISCUSSION

Taguchi's loss function is used to calculate the deviation between the experimental value and the desired value [Gaitonde et al., 2006, Carou et al., 2014]. Then the value of this function is converted to the signal-to-noise (S/N) ratio. Taguchi's philosophy comprises three general approaches to assessing the relationship between quality and variability [Gaitonde et al., 2006, Carou et al., 2014]. There is three approach of signal-to-noise available is subject to the approach of characteristics. These are 'Nominal is better approach', 'Smaller is better approach' and 'Larger is better approach' [Phadke, 1989]. In this study, the smallest optimal value of surface roughness was selected for the signal-to-ratio of better performances of factors. 'Smaller is better approach' was calculated by the following equation (1). S/N ratios of surface roughness is shown in Table 4. and their main effects plot are demonstrated in Fig. 5.

$$S/N = -10\log\left(\frac{1}{N}\left(\sum_{i=1}^{n} Y_i^2\right)\right) \qquad (1)$$

$Y_i$ is the value of surface roughness for first equation (1) for the $i^{th}$ test, n the number of tests and N the total number of data points.

In this study, the effect of the number of passes, burnishing force, burnishing speed, feed rate has been researched on surface roughness. The data acquired by applying the ball burnishing process are shown in Table 4.

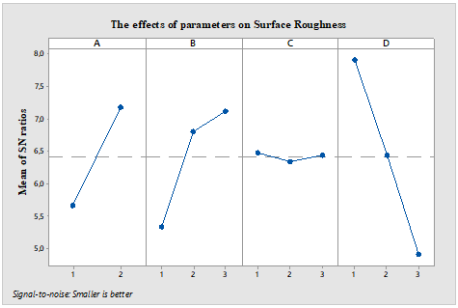


Fig. 5. The effects of parameters on Surface Roughness

Table 4. Process Parameters and Experimental results after ball burnishing process

| Experiment Number | Process Parameters | | | | Experimental Results | S/N ratio (dB) |
|---|---|---|---|---|---|---|
| | (A) Number of passes | (B) Burnishing Force | (C) Burnishing Speed | (D) Feed rate | Ra (µm) | Ra (µm) |
| 1 | 1 | 50 | 200 | 0.1 | 0.481 | 6.36 |
| 2 | 1 | 50 | 400 | 0.25 | 0.631 | 3.99 |
| 3 | 1 | 50 | 600 | 0.5 | 0.718 | 2.88 |
| 4 | 1 | 150 | 200 | 0.1 | 0.434 | 7.25 |
| 5 | 1 | 150 | 400 | 0.25 | 0.519 | 5.70 |
| 6 | 1 | 150 | 600 | 0.5 | 0.550 | 5.19 |
| 7 | 1 | 250 | 200 | 0.25 | 0.448 | 6.97 |
| 8 | 1 | 250 | 400 | 0.5 | 0.559 | 5.05 |
| 9 | 1 | 250 | 600 | 0.1 | 0.424 | 7.45 |
| 10 | 2 | 50 | 200 | 0.5 | 0.599 | 4.44 |
| 11 | 2 | 50 | 400 | 0.1 | 0.402 | 7.90 |
| 12 | 2 | 50 | 600 | 0.25 | 0.480 | 6.38 |
| 13 | 2 | 150 | 200 | 0.25 | 0.407 | 7.80 |
| 14 | 2 | 150 | 400 | 0.5 | 0.508 | 5.88 |

| | | | | | | |
|---|---|---|---|---|---|---|
| 15 | 2 | 150 | 600 | 0.1 | 0.358 | 8.93 |
| 16 | 2 | 250 | 200 | 0.5 | 0.504 | 5.95 |
| 17 | 2 | 250 | 400 | 0.1 | 0.336 | 9.47 |
| 18 | 2 | 250 | 600 | 0.25 | 0.409 | 7.76 |

Table 5. ANOM for surface roughness based on S/N

| Factors | | Level | | | Optimum level |
|---|---|---|---|---|---|
| | | 1 | 2 | 3 | |
| A | Number of passes | 5.653 | 7.172 | - | 2 |
| B | Burnishing Force (N) | 5.330 | 6.795 | 7.113 | 3 |
| C | Burnishing Speed (rpm) | 6.467 | 6.338 | 6.434 | 1 |
| D | Feed rate (mm/min) | 7.897 | 6.437 | 2.994 | 1 |

Table 6. ANOVA for surface roughness based on S/N ratio

| Parameter code | Degrees of freedom | Sum of squares | Mean squares | % Contribution |
|---|---|---|---|---|
| A | 1 | 10.3844 | 10.3844 | 20.65 |
| B | 2 | 10.8565 | 5.4282 | 21.59 |
| C | 2 | 0.0535 | 0.0268 | 0.11 |
| D | 2 | 26.8890 | 13.4445 | 53.47 |
| Error | 10 | 2.1017 | 0.2102 | |
| Total | 17 | 50.2852 | | |

The analysis of means (ANOM) based on S/N ratio was performed to decide the optimal levels of factors, the sum is shown in Table 5. The level of a control factor with the highest S/N ratio is the optimal level. The best combination control factor setting is A2, B3, C1 and D1 for minimum surface roughness.

ANOVA based on S/N ratio has been performed to know the relative importance of each of the control factors. Table 6 present the results of ANOVA for surface roughness. From ANOVA, it is observed that number of passes (20.65%), burnishing force (21.59%) and feed rate (53.47%) play significant roles in minimizing the surface roughness; while there is almost no effect of burnishing speed.

As shown in Fig. 7a., when the feed rate raises up, the surface roughness is increasing. As the burnishing force raise up, the surface roughness is decreasing. It appears that to have no change in the surface roughness results, considering the experiments the burnishing force range of 150 N to 250 N at 0.1 mm/min feed rate. Fig. 7a. exhibits that the notable parameters effect of surface roughness is feed rate and burnishing force.

As it is seen the Fig. 7b., the effect of burnishing force couldn't be significantly observed on the surface roughness. However, the burnishing force (400 rpm and 600 rpm) increases with decrease the surface roughness except to 200 rpm. As the burnishing speed increases the surface roughness increases.

As indicated in Fig. 8a., the burnishing speed increases with increase the microhardness. When the burnishing force increases from 50 N to 150 N the microhardness decreases but it increases from 150 N to 250 N. Besides, the feed rate increases with increase the microhardness. When the feed rate increases from 0.1 mm/min to 0.25 mm/min the microhardness decreases but it increases from 0.25 mm/min to 0.5 mm/min (Fig. 8b.).

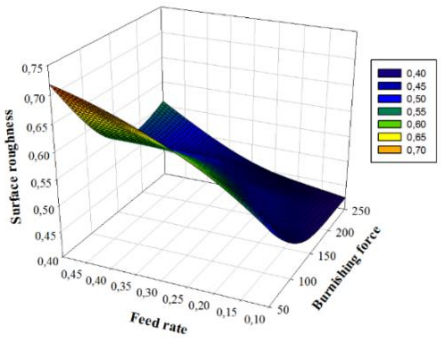


(a)

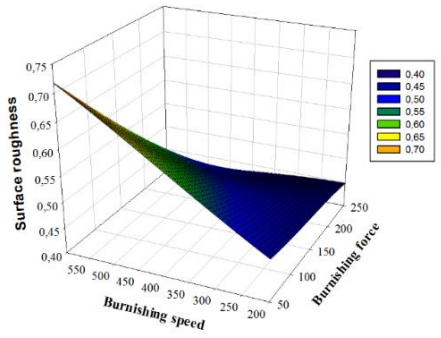


(b)

Fig. 7. a) Effect of burnishing force and feed rate on surface roughness b) Effect of burnishing speed and burnishing force on surface roughness

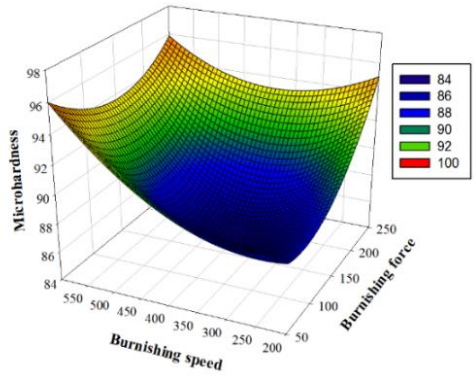


(a)

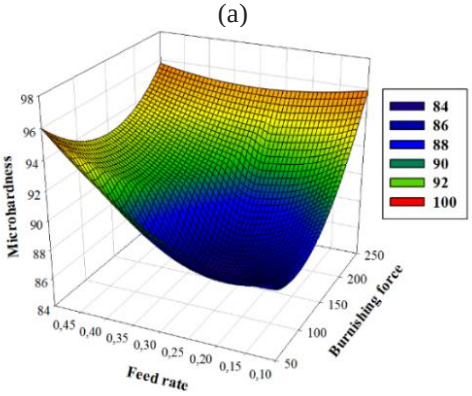


(b)

Fig. 8. a) Effect of burnishing speed and burnishing force on surface roughness b) Effect of feed and burnishing force on surface roughness

## 4. CONCLUSION

In this paper, the effect of the number of passes, burnishing force, burnishing speed and feed rate was researched on surface roughness. Taguchi method was used for optimization of these parameters, assisted in the optimization process. Conclusions from present research are given below;

• The optimal parameter combination for the minimum surface finish was obtained by using the analysis of signal-to-noise ratio. The combination of parameters and their levels for optimum surface roughness is A2B3C1D1.

• Generally, the surface roughness increases with increased feed rate. The effect of burnishing force couldn't significantly observe on the surface roughness. Also, the surface roughness decreases with increased number of passes.

• The best surface roughness value was obtained at two passes as a number of passes, 250 N burnishing force, 400 rpm burnishing speed and 0.1 mm/min feed rate settings.

• ANOVA based on S/N ratio has been performed to know the relative importance of each of the control factors. From ANOVA, it is observed that number of passes (20.65%), burnishing force (21.59%) and feed rate (53.47%) play significant roles in minimizing the surface roughness; while there is almost no effect of burnishing speed.

• From ANOVA, the results indicate that the control factors such as number of passes, burnishing force, burnishing speed and feed rate have a significant effect on surface roughness at a reliability level of 95.82%.

## REFERENCES

Buldum, B.B. (2013). Analyzing the Machinability of Magnesium Alloy. AZ91. PhD Thesis, Gazi University, Ankara, Turkey.

Buldum, B.B., Sik, A., Ozkul, I. (2013) "Investigation of magnesium alloys machinability." *International Journal of Electronics, Mechanical and Mechatronics Engineering*, Vol. 2, pp. 261-268.

Carou, D., Rubio, E.M., Lauro, C.H., Davim J P. (2014). "Experimental investigation on surface finish during intermittent turning of UNS M11917 magnesium alloy under dry and near dry machining conditions." *Measurement*, Vol. 56, pp.136-154.

Cicek, A., Kivak, T., Ekici, E. (2015). "Optimization of drilling parameters using taguchi technique and response surface methodology (RSM) in drilling of AISI 304 steel with cryogenically treated HSS drills." *Journal of Intelligent Manufacturing*, Vol. 26, pp. 295-305.

Dabeer, P.S., Purohit, G.K. (2010). "Effect of ball burnishing parameters on surface roughness using surface roughness methodology." *Advances in Production & Management*, Vol. 5, pp. 111-116.

El-Axir, M.H., Othman, O.M., Abodiena, A.M. (2008). "Improvements in out-of-roundness and microhardness of inner surfaces by internal ball burnishing process." *Journal of Materials Processing Technology*, Vol. 196, pp. 120-128.

Esme, U. (2010). "Use of grey based taguchi method in ball burnishing process for the optimization of surface roughness and microhardness of AA 7075 aluminum alloy." *Materials and Technology*, vol. 44, pp. 129-135.

El-Taweel, T.A., El-Axir, M.H. (2009). "Analysis and optimization of the ball burnishing process through the taguchi technique." *The International Journal of Advanced Manufacturing Technology*, Vol. 41, pp. 301-310.

Gaitonde, V.N., Karnik, S.R., Achyutha, B.T., Siddeswarappa, B. (2006). "Multi-response optimization in drilling using taguchi's quality loss function." *Indian Journal of Engineering and Materials Sciences*, Vol. 13, pp. 484-488.

Gnedenkov, A.S., Sinebryukhov, S.L., Mashtalyar, D.V., Gnedenkov, S.V. (2013) "Features of the corrosion processes development at the magnesium alloys surface." *Surface & Coating Technology*, Vol. 225, 112-118.

Gokce, B. (2015) "Analysis of wear behaviours of borided 440C steels by using taguchi method." *Journal of the Balkan Tribological Association*, Vol. 21, pp. 831-841.

Grzesik W, Zak K. (2012) "Modification of surface finish produced by hard turning using superfinishing and

burnishing operations." *Journal of Materials Processing Technology,* Vol. 212, pp. 315-322.

Hamamci, M., Topal, E.S. (2014). "Optimization of cutting parameters for surface roughness in CNC turning machining with aluminum alloy 6061 material." *International organization of Scientific Research,* Vol. 4, pp. 1-10.

Ibrahim, A.A., Abd Rabbo, S.M., El-Axir, M.H., Ebied, A.A. (2009). "Center rest balls burnishing parameters adaptation of steel components using fuzzy logic." *Journal of Materials Processing Technology*, Vol. 209, pp. 2428-2435.

Kayali, Y., Gokce, B., Mertgenc, E., Colak. F., Kara. R. (2013). "Analysis of wear behaviour of borided AISI 52100 steel with the taguchi method." *Journal of the Balkan Tribological Association*, Vol. 19, pp. 365-376.

López de Lacalle, L.N., Lamikiz, A., Muñoa, J., Sánchez, J.A. (2005). "Quality improvement of ball-end sculptured surfaces by ball burnishing." International Journal of Machine Tools and Manufacture, Vol. 45, pp. 1659-1668.

Low, K.O., Wong, K.J. (2011). "Influence of ball burnishing on surface quality and tribological characteristics of polymers under dry sliding conditions." *Tribology International*, Vol. 44, pp. 44-153.

Luca, L., Neagu-Ventzel, S., Marinescu, I. (2005). "Effects of working parameters on surface finish in ball-burnishing of hardened steels." *Precision Engineering*, Vol. 29, pp. 253–256.

Mahajan D, Tajane R. (2013). "A review on ball burnishing process". *International Journal of Scientific and Research Publications*, Vol. 3, pp. 1-8.

Oktem, H., Erzurumlu, T., Col, M. (2006) "A study of the taguchi optimization method for surface roughness in finishing milling of mold surfaces." *The International Journal of Advanced Manufacturing Technology*, Vol. 28, pp. 694-700.

Phadke, M.S. (1989). *Quality engineering using robust design*. Prentice Hill, New York, USA.

Pishbin, F., Simchi, A., Ryan, P., Boccaccini, A.R. (2010). "A study of the electrophoretic deposition of bioglass suspensions using the taguchi experimental design approach." *Journal of the European Ceramic Society*, Vol.30, pp. 2963-2970.

Rodriguez, A., Lopez de Lacelle, L.N., Celaya, A., Lamikiz, A., Albizuri, J. (2010). "Surface improvement of shafts by the deep ball-burnishing technique." *Surface & Coatings Technology*, Vol. 206, pp. 2817-2824.

Sagbas, A. (2011) "Analysis and optimization of surface roughness in the ball burnishing process using response surface methodology and desirability function." *Advances in Engineering Software*, Vol. 42, pp. 992-998.

Thamizhmnaii, S., Omar, B.B., Saparudin, S., Hasan, S. (2008). "Surface roughness investigation and hardness by burnishing on titanium alloy." *Journal of Achievements in Materials and Manufacturing Engineering*, Vol. 28, pp. 139-142.

Tian, Y., Shin, Y.C. (2007). "Laser-assisted burnishing of metals." *International Journal of Machine Tools & Manufacture*, Vol. 47, pp. 14-22.

Zhang, P., Lindemann, J. (2005). "Influence of shot peening on high cycle fatigue properties of the high-strength wrought magnesium alloy AZ80." *Scripta Materialia*, Vol. 52, pp. 485–490.

# Turkish Journal of Engineering

*Turkish Journal of Engineering (TUJE)*
*Vol. 1, Issue 1, pp. 32-36, May 2017*
*ISSN 2587-1366, Turkey*
*DOI: 10.31127/tuje.316683*
*Research Article*


## pH CHANGE IN ELECTROCHEMICAL OXIDATION OF IMIDACLOPRID PESTICIDE USING BORON-DOPED DIAMOND ELECTRODES


Bahadır K. Körbahti *[1] and M. Ceyhun Erdem [2]

[1] Mersin University, Faculty of Engineering, Chemical Engineering Department, Mersin, Turkey
(korbahti@mersin.edu.tr)

[2] Mersin University, Faculty of Engineering, Chemical Engineering Department, Mersin, Turkey
(mceyhunerdem@gmail.com)

* Corresponding Author


Received: 08/04/2017 Accepted: 05/05/2017



**ABSTRACT**

In this study, pH and ΔpH change in the electrochemical oxidation of imidacloprid (IMD) pesticide using boron-doped diamond (BDD) electrodes was investigated in the presence of $Na_2SO_4$ electrolyte. The process parameters were operated as imidacloprid concentration (40-200 mg/L), electrolyte concentration (2-10 g/L), current density (4-20 mA/cm$^2$) and reaction temperature (20-60°C). pH and ΔpH values increased with increasing $Na_2SO_4$ concentration, current density, and reaction temperature, and decreasing the imidacloprid concentration at 120 min reaction time. The results of this study showed that the pH of the wastewater solution maintained the local pH discharge limits between 6 and 9 after the electrochemical oxidation.



***Keywords:*** *BDD, Boron-doped diamond electrode, Electrolysis, Imidacloprid, Pesticide, Wastewater treatment*

## 1. INTRODUCTION

The use of pesticides is increasing with growing of world population due to the increase in food demand. Pesticides have become an integral part of the agricultural production all over the world since 20th century in increasing the productivity of plants, the quality of agricultural products, and preventing diseases spread with the insects (Galt, 2008; Bouya *et al*., 2012). However, overconsumption and improper use may cause chemical segregation and ecological damages to the environment (Bouya *et al*., 2012). Uncontrolled consumption of pesticides may cause water, soil and air pollution; and harmful organisms can gain resistance to the pesticides (Bouya *et al*., 2012). Pesticide residues are being contaminating water resources by direct contact with plants or insects in water or on the waterside, by washing soil surfaces or plants by rainwater, and by discharging pharmaceutical industry wastewater to the aquatic environment (Bouya *et al*., 2012).

In order to prevent such risks, many laws were issued in EU countries and in the USA (Gullino *et al*., 1994). In the literature, electrochemical oxidation of 2,4-D, 2,6-D, diazinon, melathion, chloropyrifos, azinphosmethyl, phorate, paraquat, atrazine, thiram, parathion methyl, 2,4-DNP, dichlorvos, myclobutanil, triadimefon and propiconazole pesticides were investigated (Souza *et al*., 2016; Fontmorin *et al*., 2015; Madsen *et al*., 2015; Lazarević-Pašti *et al*., 2012; Cartaxo *et al*., 2015; Steter *et al*., 2016; Malpass *et al*., 2006; Arapoglou *et al*., 2003; Vargas *et al*., 2014; Quiroz *et al*., 2014; Urzúa *et al*., 2013).

It is very important that the wastewater solution should maintain the discharge limits after the treatment. The local pH discharge limit in Turkey is between 6 and 9. Therefore, the pH of the solution should be maintained between 6 and 9 after the treatment. In this study, the effect of process parameters such as imidacloprid concentration, electrolyte concentration, current density and reaction temperature was investigated on pH and ΔpH change in electrochemical oxidation of imidacloprid (IMD) pesticide using boron-doped diamond (BDD) electrodes in the presence of $Na_2SO_4$ electrolyte. The optimum operating region was determined in order to maintain the local pH discharge limits.

## 2. MATERIALS AND METHODS

Imidacloprid (IMD) pesticide obtained from Astranova (Turkey) as a concentrated emulsion (350 g/L) and diluted to 40-200 mg/L using double distilled water. Double distilled water was produced using Millipore Simplicity® UV ultrapure water system and GFL-2008 water still. Batch reactor system consists of electrochemical reactor with heating/cooling jacket, Lauda RE 630 S cryostat water bath, Heidolph RZR 2021 mechanical mixer, Goodwill PST-3201 programmable DC power source and Heidolph PD 5206 peristaltic pump. Boron-doped diamond (Nb/BDD) electrodes (CONDIAS, Germany) were used as anode and cathode materials. Total electrode surface area was 260 $cm^2$. Samples in 10 mL volume were withdrawn from the reaction medium at 5 min time intervals for the analysis. pH was measured using WTW inoLab BNC720 pH meter.

## 3. RESULTS AND DISCUSSION

In electrochemical treatment processes, organic pollutants could be removed from wastewater by indirect and direct mechanisms (Brillas and Martínez-Huitle, 2015; Comninellis and Chen, 2010; Körbahti and Artut K, 2010; Körbahti and Taşyürek, 2015; Panizza and Cerisola, 2009). Indirect oxidation occurs in the liquid bulk phase by the mediated oxidants, and direct oxidation at the anode surface (Brillas and Martínez-Huitle, 2015; Comninellis and Chen, 2010; Körbahti and Artut K, 2010; Körbahti and Taşyürek, 2015; Panizza and Cerisola, 2009). Most electrochemical processes are based on indirect oxidation because direct oxidation of organic pollutants are very slow on inert anodes due to the limiting reactions and reaction kinetics (Tarr, 2003; Rajeshwar and Ibanez, 1997).

Boron-doped diamond (BDD) thin-film anodes have better $O_2$ overpotential than the conventional anodes. Therefore, more hydroxyl radicals adsorb on the electrode surface and organic compounds degrade faster (Comninellis and Chen, 2010; Cañizares *et al*., 2006; Siné *et al*., 2005). Hydroxyl radicals produce by the anodic discharge of water in indirect electrochemical oxidation at BDD anodes. Hydroxyl radicals are not selective for the degradation of organic pollutants (R) that they react with the organic pollutants (R), and mineralize into $CO_2$ and $H_2O$ (Comninellis and Chen, 2010; Cañizares *et al*., 2006; Siné *et al*., 2005).

$$\boldsymbol{BDD + H_2O \longrightarrow BDD(^{\bullet}OH) + H^+ + e^-} \quad (1)$$

$$\boldsymbol{BDD(^{\bullet}OH) + R \longrightarrow BDD + CO_2 + H_2O} \quad (2)$$

In this study, the process parameters were operated as imidacloprid concentration (40-200 mg/L), $Na_2SO_4$ concentration (2-10 g/L), current density (4-20 $mA/cm^2$) and reaction temperature (20-60°C) in electrochemical oxidation of imidacloprid (IMD) pesticide using boron-doped diamond (BDD) electrodes. pH and ΔpH change monitored during the electrochemical oxidation and the results are presented in Figures 1 and 2.

Figure 1 (A)-(D) shows the effect of process parameters on pH change. pH values decreased to acidic region in 30 min from the beginning for all runs and then increased to the basic region during the electrochemical oxidation. pH values were increased from their initial value with increasing $Na_2SO_4$ concentration, current density, and reaction temperature, and decreasing the imidacloprid concentration at 120 min reaction time. pH of the reaction medium decreased from 9.9 to 5.4 with increasing IMD concentration from 40 mg/L to 200 mg/L. Electrolyte type and concentration are important parameters in electrochemical processes that increase or decrease the process efficiency due to the formation of intermediate derivatives (Palma-Goyes *et al*, 2010). Increasing $Na_2SO_4$ from 2 g/L to 10 g/L, increased pH of the reaction medium from 4.7 to 9.8. In the literature, it was reported that the reaction between hydroxyl radicals and organic contaminants accelerates and removal efficiency increases with increasing the current density and reaction temperature (Brillas *et al*., 2005). pH of the reaction medium increased from 3.9 to 10 with increasing the current density from 4 $mA/cm^2$ to 20 $mA/cm^2$. Increasing reaction temperature from 20°C to 60°C slightly increased the pH of the reaction medium from 8.0 to 8.9.

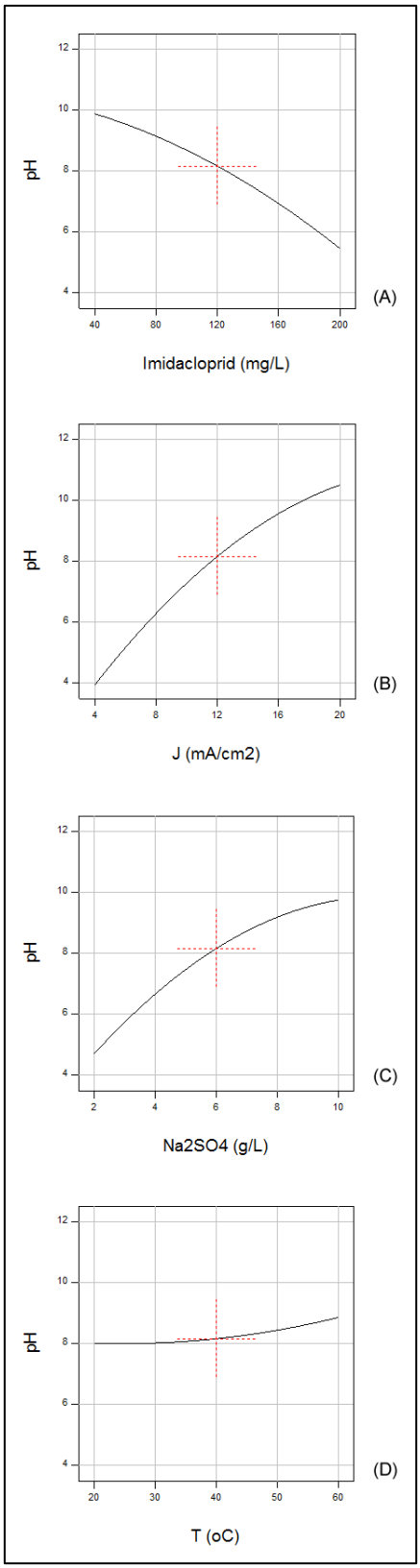


Figure 1. Effect of process parameters on pH change (A) J=12 mA/cm$^2$, $Na_2SO_4$=6 g/L, T=40°C, t=120 min; (B) $C_{IMD,o}$=120 mg/L, $Na_2SO_4$=6 g/L, T=40°C, t=120 min; (C) $C_{IMD,o}$=120 mg/L, J=12 mA/cm$^2$, T=40°C, t=120 min; (D) $C_{IMD,o}$=120 mg/L, J=12 mA/cm$^2$, $Na_2SO_4$=6 g/L, t=120 min.

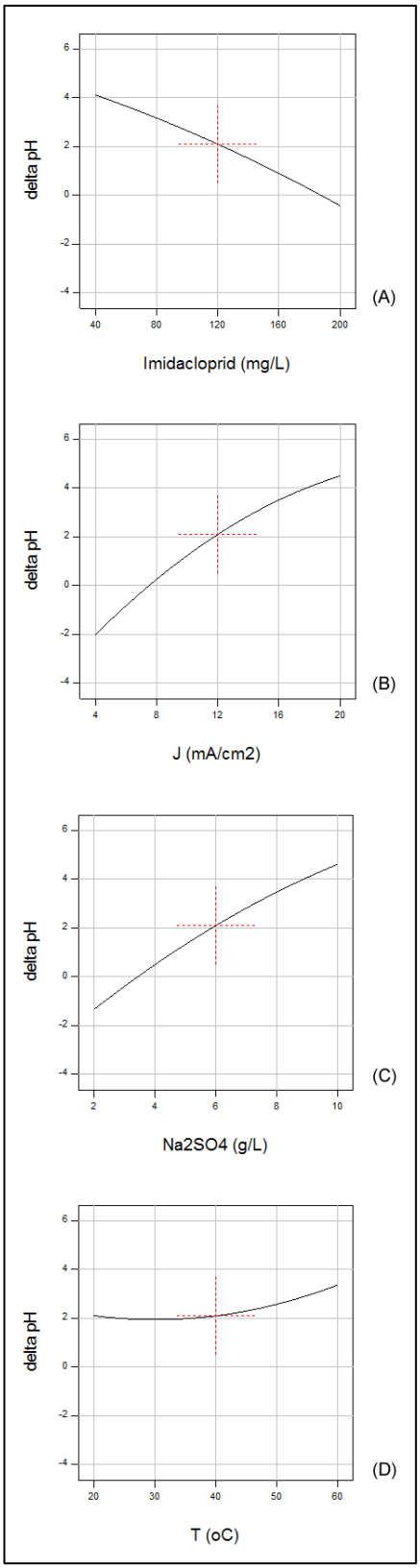


Figure 2. Effect of process parameters on ΔpH change (A) J=12 mA/cm$^2$, $Na_2SO_4$=6 g/L, T=40°C, t=120 min; (B) $C_{IMD,o}$=120 mg/L, $Na_2SO_4$=6 g/L, T=40°C, t=120 min; (C) $C_{IMD,o}$=120 mg/L, J=12 mA/cm$^2$, T=40°C, t=120 min; (D) $C_{IMD,o}$=120 mg/L, J=12 mA/cm$^2$, $Na_2SO_4$=6 g/L, t=120 min.

The optimum operating region for pH between 6.0 and 9.0 at 120 min reaction time were determined from Figure 1 (A)-(C) at 85-186 mg/L IMD concentration, 3.3-7.7 g/L $Na_2SO_4$ concentration, 7.5-14.3 mA/cm$^2$ current density and 20-60°C reaction temperature.

The effect of process parameters on ΔpH change can be seen in Figure 2 (A)-(D). ΔpH values were calculated using Equation 3. In Equation 3, $pH_i$ is the initial pH value of the reaction medium and $pH_f$ is the final pH value at 120 min.

$$\Delta \boldsymbol{pH} = \boldsymbol{pH_f} - \boldsymbol{pH_i} \quad (3)$$

$\Delta \boldsymbol{pH} < \boldsymbol{0}$ indicates $\boldsymbol{pH_f} < \boldsymbol{pH_i}$, $\Delta \boldsymbol{pH} = \boldsymbol{0}$ indicates $\boldsymbol{pH_f} = \boldsymbol{pH_i}$, and $\Delta \boldsymbol{pH} > \boldsymbol{0}$ indicates $\boldsymbol{pH_f} > \boldsymbol{pH_i}$. ΔpH values were increased with increasing $Na_2SO_4$ concentration, current density, and reaction temperature, and decreasing the imidacloprid concentration at 120 min reaction time. ΔpH of the reaction medium decreased from +4.1 to -0.4 with increasing IMD concentration from 40 mg/L to 200 mg/L. Increasing $Na_2SO_4$ from 2 g/L to 10 g/L, increased ΔpH from -1.4 to +4.6. ΔpH increased from -2.0 to +4.5 with increasing the current density from 4 mA/cm$^2$ to 20 mA/cm$^2$. Increasing reaction temperature from 20°C to 60°C slightly increased the ΔpH of the reaction medium from +2.0 to +3.4.

The point for ΔpH = 0 at 120 min reaction time were determined at 188 mg/L IMD concentration, 3.5 g/L $Na_2SO_4$ concentration and 7.6 mA/cm$^2$ current density from Figure 2 (A)-(C).

The electrolysis of an aqueous solution of sodium sulphate using inert electrodes produces hydrogen at the cathode and oxygen at the anode. Hydrogen ions are being removed from solution and leaving an excess of hydroxyl ions which makes the solution alkaline at the cathode, and hydroxyl ions are being removed and leaving an excess of hydrogen ions which makes the solution acidic at the anode (Comninellis and Chen, 2010).

## 4. CONCLUSION

In this study, pH and ΔpH change in the electrochemical oxidation of imidacloprid (IMD) pesticide using boron-doped diamond (BDD) electrodes was investigated in the presence of $Na_2SO_4$ electrolyte. pH and ΔpH values increased with increasing $Na_2SO_4$ concentration, current density, and reaction temperature, and decreasing the imidacloprid concentration at 120 min reaction time. pH values decreased to acidic region in 30 min from the beginning for all runs and then increased to the basic region during the electrochemical oxidation. It can be concluded that pH decreased due to the production of hydroxyl radicals at the BDD anode and oxygen evolution reaction. pH of the reaction medium increased to the alkaline region while these reactions are getting slower during electrochemical oxidation. The optimum operating region for pH between 6.0 and 9.0 at 120 min reaction time were determined at 85-186 mg/L IMD concentration, 3.3-7.7 g/L $Na_2SO_4$ concentration, 7.5-14.3 mA/cm$^2$ current density and 20-60°C reaction temperature. The results of this study showed that the pH of the wastewater solution maintained the local pH discharge limits between 6 and 9 after the electrochemical oxidation, being an advantage for the neutralization of treated wastewater without using any chemicals.

## ACKNOWLEDGEMENTS

This project was supported by Mersin University Scientific Research Projects Center (MEÜ BAP) with Grant No. 2016-1-TP2-1393.

## REFERENCES

Arapoglou, D., Vlyssides, A., Israilides, C., Zorpas, A. and Karlis, P. (2003). "Detoxification of methyl-parathion pesticide in aqueous solutions by electrochemical oxidation". *Journal of Hazardous Materials*, Vol. 98, No. 1-3, pp. 191-199.

Brillas, E. and Martínez-Huitle, C.A. (2015). "Decontamination of wastewaters containing synthetic organic dyes by electrochemical methods. An updated review". *Applied Catalysis B: Environmental*, Vol. 166-167, pp. 603-643.

Brillas, E., Sirés, I., Arias, C., Cabot, P.L., Centellas, F., Rodríguez, R.M. and Garrido, J.A. (2005). "Mineralization of paracetamol in aqueous medium by anodic oxidation with a boron-doped diamond electrode". *Chemosphere*, Vol. 58, No. 4, pp. 399-406.

Cañizares, P., Sáez, C., Lobato, J. and Rodrigo, M.A. (2006). "Detoxification of synthetic industrial wastewaters using electrochemical oxidation with boron-doped diamond anodes". *Journal of Chemical Technology & Biotechnology*, Vol. 81, No. 3, pp. 352-358.

Cartaxo, M.A.M., Borges, C.M., Pereira, M.I.S. and Mendonça, M.H. (2015). "Electrochemical oxidation of paraquat in neutral medium". *Electrochimica Acta*, Vol. 176, pp. 1010-1018.

Comninellis, Ch. and Chen, G. (2010). *Electrochemistry for the Environment*, Springer, USA.

Fontmorin, J.M., Fourcade, F., Geneste, F., Soutrel, I., Floner, D. and Amrane, A. (2015). "Direct electrochemical oxidation of a pesticide, 2,4-dichlorophenoxyacetic acid, at the surface of a graphite felt electrode: Biodegradability improvement". *Comptes Rendus Chimie*, Vol. 18, No. 1, pp. 32-38.

Galt, R.E. (2008). "Beyond the circle of poison: Significant shifts in the global pesticide complex, 1976-2008". *Global Environmental Change*, Vol. 18, No. 4, pp. 786-799.

Gullino, M.L. and Kuijpers, L.A.M. (1994). "Social and Political Implications of Managing Plant Diseases with Restricted Fungicides in Europe". *Annual Review of Phytopathology*, Vol. 32, No. 1, pp. 559-581.

Körbahti, B.K. and Artut, K. (2010). "Electrochemical oil/water demulsification and purification of bilge water using Pt/Ir electrodes". *Desalination*, Vol. 258, No. 1-3, pp. 219-228.

Körbahti, B.K. and Taşyürek, S. (2015). "Electrochemical oxidation of ampicillin antibiotic at boron-doped diamond electrodes and process optimization using response surface methodology". *Environmental Science and Pollution Research*, Vol. 22, No. 5, pp. 3265-3278.

Lazarević-Pašti, T.D., Bondžić, A.M., Pašti, I.A. and Vasić, V.M. (2012). "Indirect electrochemical oxidation of organophosphorous pesticides for efficient detection via acetylcholinesterase test". *Pesticide Biochemistry and Physiology*, Vol. 104, No. 3, pp. 236-242.

Madsen, H.T., Søgaard, E.G. and Muff, J. (2015). "Study of degradation intermediates formed during electrochemical oxidation of pesticide residue 2,6-dichlorobenzamide (BAM) in chloride medium at boron doped diamond (BDD) and platinum anodes". *Chemosphere*, Vol. 120, pp. 756-763.

Malpass, G.R.P., Miwa, D.W., Machado, S.A.S., Olivi, P. and Motheo, A.J. (2006). "Oxidation of the pesticide atrazine at DSA® electrodes". *Journal of Hazardous Materials*, Vol. 137, No. 1, pp. 565-572.

Palma-Goyes, R.E., Guzmán-Duque, F.L., Peñuela, G., González, I., Nava, J.L. and Torres-Palma, R.A. (2010). "Electrochemical degradation of crystal violet with BDD electrodes: Effect of electrochemical parameters and identification of organic by-products". *Chemosphere*, Vol. 81, No. 1, pp. 26-32.

Panizza, M. and Cerisola, G. (2009). "Direct and Mediated Anodic Oxidation of Organic Pollutants". *Chemical Reviews*, Vol. 109, No. 12, pp. 6541-6569.

Quiroz, M.A., Sánchez-Salas, J.L., Reyna, S., Bandala, E.R., Peralta-Hernández, J.M. and Martínez-Huitle, C.A. (2014). "Degradation of 1-hydroxy-2,4-dinitrobenzene from aqueous solutions by electrochemical oxidation: Role of anodic material". *Journal of Hazardous Materials*, Vol. 268, pp. 6-13.

Rajeshwar, K. and Ibanez, J.G. (1997). *Environmental Electrochemistry*, Academic Press, USA.

Siné, G. and Comninellis, Ch. (2005). "Nafion®-assisted deposition of microemulsion-synthesized platinum nanoparticles on BDD". *Electrochimica Acta*, Vol. 50, No. 11, pp. 2249-2254.

Souza, F.L., Saéz, C., Lanza, M.R.V., Cañizares, P. and Rodrigo, M.A. (2016). "Removal of pesticide 2,4-D by conductive-diamond photoelectrochemical oxidation". *Applied Catalysis B: Environmental*, Vol. 180, pp. 733-739.

Steter, J.R., Kossuga, M.H. and Motheo, A.J. (2016). "Mechanistic proposal for the electrochemical and sonoelectrochemical oxidation of thiram on a boron-doped diamond anode". *Ultrasonics Sonochemistry*, Vol. 28, pp. 21-30.

Tarr, M.A. (2003). *Chemical Degradation Methods for Wastes and Pollutants*, CRC Press, USA.

Urzúa, J., González-Vargas, C., Sepúlveda, F., Ureta-Zañartu, M.S. and Salazar, R. (2013). "Degradation of conazole fungicides in water by electrochemical oxidation". *Chemosphere*, Vol. 93, No. 11, pp. 2774-2781.

Vargas, R., Díaz, S., Viele, L., Núñez, O., Borrás, C., Mostany, J. and Scharifker, B.R. (2014). "Electrochemical oxidation of dichlorvos on $SnO_2$-$Sb_2O_5$ electrodes". *Applied Catalysis B: Environmental*, Vol. 144, pp. 107-111.

# Turkish Journal of Engineering

*Turkish Journal of Engineering (TUJE)*
*Vol. 1, Issue 1, pp. 37-43, May 2017*
*ISSN 2587-1366, Turkey*
*DOI: 10.31127/tuje.320047*
*Research Article*

## DETERMINATION OF OPTIMUM MESH SIZE TO MEASURE TOOTH ROOT STRESS OF SPUR GEAR USING FINITE ELEMENT ANALYSIS

Ömer Uçtu *[1], İbrahim Sevim [2], Bülent Karataş [3] and Burak Şahin [4]

[1] Mersin University, Faculty of Engineering, Mechanical Engineering Department, Mersin, Turkey
(omeructu@outlook.com)

[2] Mersin University, Faculty of Engineering, Mechanical Engineering Department, Mersin, Turkey
(ibrahimsevim33@gmail.com)

[3] Harran University, Faculty of Engineering, Mechanical Engineering Department, Şanlıurfa, Turkey
(bulent.karatas@bcsmetal.com.tr)

[4] Gaziantep University, Faculty of Engineering, Mechanical Engineering Department, Gaziantep, Turkey
(buraksahin@gantep.edu.tr)

* Corresponding Author
Received: 09/04/2017 Accepted: 06/05/2017

**ABSTRACT**
Gears are one of the most important power transmission elements. High speed gear and gear which has high loading capacity are necessary for engineering applications. Gears should be analyzed theoretically according to design criteria and tested. Theoretical analysis is generally performed by using finite element methods through simulating gears. In this study, spur gears at definite module and teeth number are modelled by Catia. They are analyzed by using SimXpert and Marc softwares for different loads on pitch circle. Tooth root bending stress values are recorded after analysis. Meshing, mesh size selection and mesh type are one of important steps for FEM. Different meshes (fine and coarse) are used for tooth root and other regions of gear profiles in this study. At tooth root, different mesh sizes are experienced and tooth root stress values are obtained. These values are compared with analytical calculation results to state optimal mesh size.

***Keywords:*** *Finite Element Analysis, Spur Gears, Mesh Size, Tooth Root Stress*

## 1. INTRODUCTION

Gears are the one of the main power transmission element. Commonly, Studies related to gears have been carried out via theoretical studies and these studies have been supported via experimental studies to evidence. Reason of this, theoretical studies have been conducted by researchers via some of presumptions and predictions. These accuracies or false of presumptions and predictions (hypothesis) have been authenticated with experimental studies. However, today high investment costs are needed for gear test rigs, equipments and instruments. Parallel to the very rapid development of technology, gears can be tested and analyzed with simulation softwares on computers very quickly. Due to this reason, the locations of expensive testing machines and equipment have been changed by simulation programs. Simulation programs mainly consists of the finite element programs. As required, finite element programs may be individual or commercial. Main purpose is which program can be supplied requires of users. Nowadays, finite element programs have been developed quickly as requires of user and these programs are compensated them easily.

Using gears on the finite element programs mainly tooth root stress, contact stress, fatigue, vibration and the others have been studied. Pawara, Utpatb (2015) studied about spur gear FEM analysis. In addition, Chena, Zhaia, Shaob, Wanga, Sunc, (2016) analyzed spur gears in Anys., If gears used in many critical applications such as automotive and aerospace sector are only studied theoretically, it requires non-possible risks confirmed by the designer and manufacturer. Due to these reasons, some countries and institutions about the development of gear design and manufacturing technology have been carried out scientific and technological R&D studies to be authenticated and controlled them many years. Main countries are USA(AGMA), Germany (FZG), England (BGA), France (CETIM), Italy and Japan. They've lost the most time during these studies while applying mesh. Reason of this is difficulties of mesh process. Researchers used the finite element program don't anticipate that they use which element type, which mesh size, mesh type and the other parameters.

In this study, Parametric spur gear are designed using Catia, and spur gear is analyzed for bending stress using finite element program to lead for the researchers in order to optimize of meshing. Researchers will not spend their time by trying different mesh types, mesh sizes, element types and other parameters due to this study. They will determine easily for future works.

## 2. MATERIAL AND METHODS

### 2.1. Spur Gear Computer Aided Design in Catia

There are many three dimensional softwares used to create spur gear geometry. Catia, Solidworks, AutoCAD, Pro-Engineer are most important and useful. In this study, parametric spur gear model is obtained by using Catia. Uctu, (2015) described the process in his master thesis in attaches. The following steps are applied to obtain spur gear geometry:

- Formulas need to create spur gear geometry are stated (Table 1). It is worked by Babu and Tsegaw (2009).

Table 1. Formulas for spur gear parametric design

| P | Formula | Description/ Units used for construction |
|---|---|---|
| a | 20deg | Pressure angle: technologic constant (10deg ≤ a ≤ 20deg) / Angular degree |
| m | — | Modulue / millimeter |
| Z | — | Number of teeth (5 ≤ Z ≤ 200) / Integer |
| p | m * π | Pitch of the teeth on a straight generative rack / millimeter |
| e | p / 2 | Circular tooth thickness, measured on the pitch circle / millimeter |
| ha | m | Addendum = height of a tooth above the pitch circle / millimeter |
| hf | if m > 1.25 hf = m * 1.25 else hf = m * 1.4 | Dedendum = depth of a tooth below the pitch circle. Proportionally greater for a small modulus (≤ 1.25 mm) / millimeter |
| rp | m * Z / 2 | Radius of the pitch circle / millimeter |
| ra | rp + ha | Radius of the outer circle / millimeter |
| rf | rp - hf | Radius of the root circle. / millimeter |
| rb | rp * cos( a ) | Radius of the base circle /millimeter |
| rc | m * 0.38 | Radius of the root concave corner. (m * 0.38) is a normative formula / millimeter |
| t | 0 ≤ t ≤ 1 | Sweep parameter of the involute curve / floating point number |
| yd | rb * ( sin(t * π) - cos(t * π) * t * π ) | Y coordinate of the involute tooth profile, generated by the t parameter / millimeter |
| zd | rb * ( cos(t * π) + sin(t * π) * t * π ) | Z coordinate of the involute tooth profile / millimeter |
| ro | rb * a * π / 180deg | Radius of the osculating circle of the involute curve, on the pitch circle / millimeter |
| c | sqrt( 1 / cos( a )$^2$ - 1 ) / PI * 180deg | Angle of the point of the involute that intersects the pitch circle / angular degree |
| phi | atan( yd(c) / zd(c) ) + 90deg / Z | Rotation angle used for making a gear symmetric to the ZX plane / angular degree |

- "Generative Shape Design" Module of Catia is opened. Then, "Parameters and Relations" (under Properties) is made active to see it in Product Tree and "With value and with Formula" is selected.
- "Formulas: Partbody (f(x))" property is used to enter gear parameters respectively. Selection of parameters type is very important. Parameter type is entered as a characteristic length for module and degree for pressure angle.
- After adding input parameters, all parameters are selected in main menu. Then in same menu, "add formula" function (Table 1) is entered. Parameters such as pitch circle radius, base radius, outside circle, root circle and fillet radius can be calculated. If they are calculated or not should be checked in product tree (Figure 1).

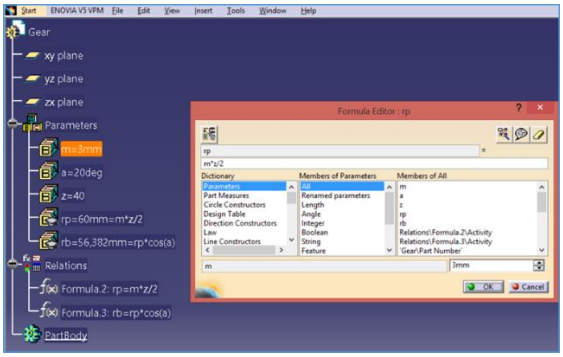


Fig. 1. Checking of Parameters

- Involute gear profile is drawn with respect to Y and Z Cartesian coordinates. Law editor in Catia window is opened by using fog icon. Then, the following path "yd > select ok > add parameters, t – select real, and x - length select their types and apply > ok" is pursued. yd equation is:

yd: yd=rb*(sin (t*PI*1rad)-cos (t*PI*1rad) * t*PI) (1)

Same procedure is applied to obtain zd. Equation of zd is:

zd: zd= rb*(cos (t*PI*1rad) +sin (t*PI*1rad) *t*PI) (2)

These equations are used to obtain involute curve. These two curves (yd and zd) combine involute curve.

- Yd(t) and Zd(t) equations are used to provide involute gear coordinates. In YZ plane, five points are obtained. The following steps are applied. The points are used to create involute by using spline command:

Insert > Wireframe> Point> Select point type: on plane>Select YZ plane > for position Y and Z, right click and Edit formula. In order to ordinate, double click the Relations\Zd. evaluate (0). Extrapolate command is used to involute is moved to gear center.

- ZX Plane is used as symmetry axis and curve is rotated for an exact angle. Before angle rotation, c parameter and formula is added (c=sqrt(1/(cos(a)*cos(a))-1)/PI). C parameter is real. For angle, "Phi =atan (Relations\yd. Evaluate(c)/Relations\zd. Evaluate(c)) +90deg/z" equation is generated and rotation is applied. Reference axis and points are hided.
- Root and tip circles are created.
- At the intersection point of root circle and involute curve, fillet is created and this fillet radius is stated as rc parameter. It is used also for next tooth of gear.
- Involute curve, tip circle diameter and fillet radius are divided by split command. The symmetry of curve is generated. The excess parts of curve are trimmed.
- Gear tooth profile is arrayed by number of teeth around gear center.
- Face width is entered to created three-dimension model.
- Tooth geometry is arrayed around the center of gear about gear numbers and linked with teeth number parameter.
- Finally, gear is padded to give thickness and finished. (Figure 2)

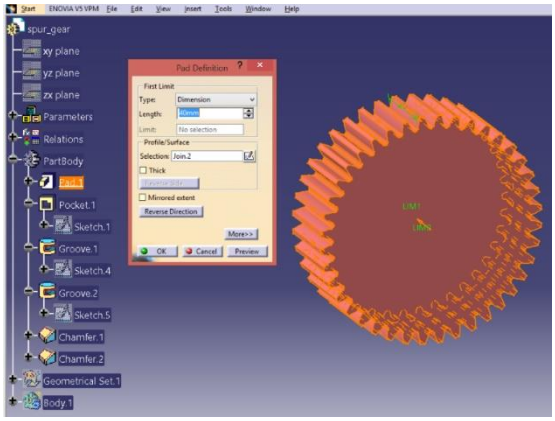


Fig. 2. Final Gear Model

## 2.2. Application of Mesh

The most important step in finite element analysis is meshing of model. The selection and application of suitable mesh provides easy analysis of models for users. Before meshing, some geometrical arrangement is made. Generally, only one tooth is analyzed by cancelling rest of gear teeth. But the result is not very accurate for one tooth application. So, three teeth model is used to analyze in this study as shown in Figure 3.

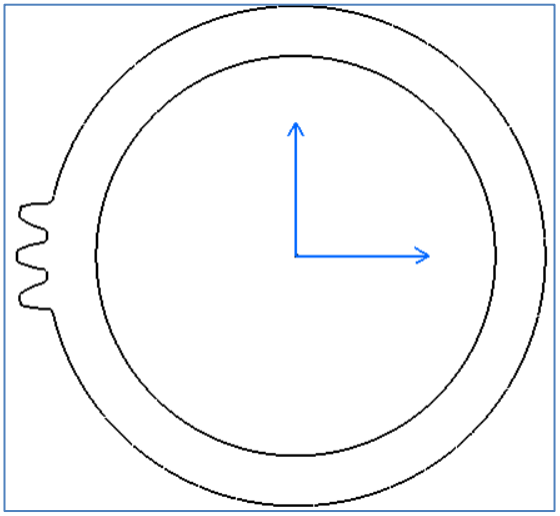

Fig. 3. Three Teeth Gear Model

In this study, Simxpert and Marc finite element software are used. These softwares have advantages and disadvantages. Meshing is easy and fast in Simxpert. Simxpert training can found guide (MSC Softwares,2015). Load application on gear is more effective in Marc. Marc training can found guide (MSC Softwares,2016). So, meshing is applied for surface in Simxpert's structure module and face width is added. Gear geometry which is loaded is offset by 2-3 mm from gear center. The reason is to apply fine mesh through involute and trochoid. Other regions are meshed less finely. Application of fine mesh for all regions on gear profile is possible but this increase analysis time. Sometimes software faults due to less performance of computer. Meshing process variables are mesh shape,

elements size and mesh method. Mesh type is not changed. Element shape is used as Quad 4 and Quad 8 (figure 4).

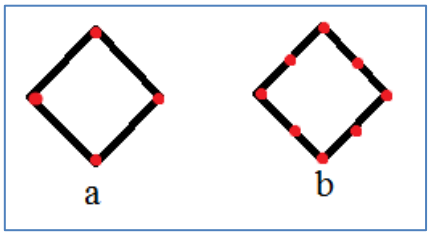


Fig. 4. Element Shape (a: Quad4, b: Quad8)

Table 2. Element Size which is studied for Mesh Size

| Element Size (mm) | **0,5** | **0,4** | **0,3** | **0,2** | **0,1** | **0,05** | **0,02** | **0,01** |
|---|---|---|---|---|---|---|---|---|

Element sizes used in analysis are given in Table 1. Meshing method are automatic mesh, and mapped mesh used in this study. Mesh model is given in Figure 5.

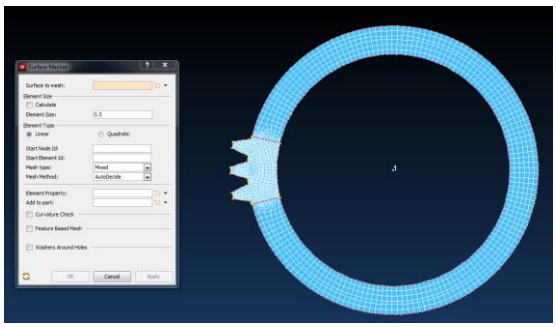

Fig. 5. Meshed Model of Gear

Applied mesh sizes between 0,5mm and 0,01mm are presented in Figure 6. After mesh application, models are saved as .bdf extension format to provide opening by Marc. For each mesh size, a new file is created.

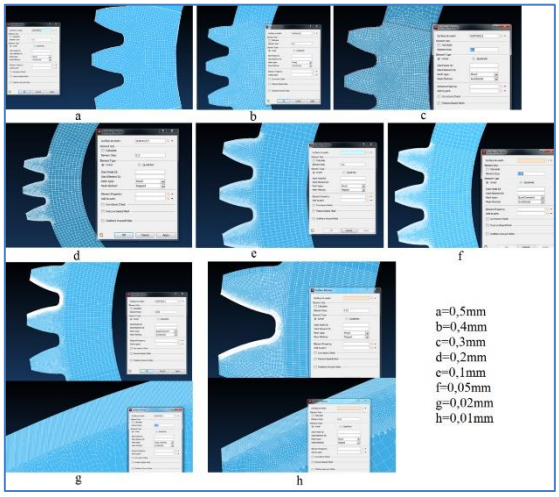


Fig. 6. Mesh Model with Their Sizes

## 2.3. Application of Loads and Analysis of Spur Gear

Another important step is application of load after meshing. This is very easy in Marc. The files created in .bdf file extension by Simxpert software can be opened easily by Marc. A point is created at the center of gear and all nodes are tightened to this point (Figure 7). This makes analysis steps easier. Then, the intersection point of pitch circle diameter and involute curve is stated. The force is applied at this point by using edge force command (Figure 8). Load application for Quad4 and Quad8 is shown in Figure 7a and 7b.

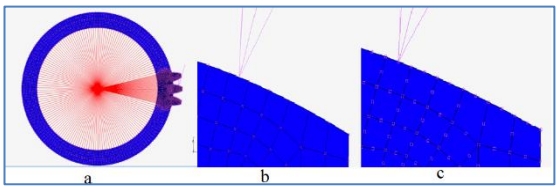


Fig. 7. Nodes Tightening (a: General view, b: Quad4, c: Quad8)

These steps are applied for other meshes respectively. Force values are given in Table 2.

Table 3. Force Values

| Force (N) | **1000** | **2000** | **3000** | **4000** | **5000** |
|---|---|---|---|---|---|

For each force value, 8 different mesh sizes and 2 different mesh shapes are used as general. For each force 16 analyses are applied. 80 different analyses are conducted for pitch point of one tooth of gear. The result of analysis for 1000N and 5000N, Quad4, 0,5mm mesh size is given in Figure 8.

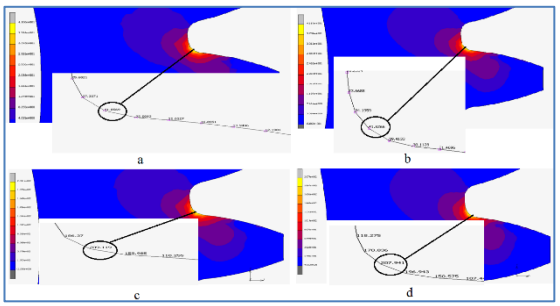


Fig. 8. Force Application (a: 1000N-Quad4, b: 1000N-Quad8, c: 5000N-Quad4, d: 5000N-Quad8)

The analysis result is given in Table 4 for 1000N and Quad4. Max gear tooth root stress is between 41,63Mpa and 43,93Mpa. Maximum stress is obtained for 0.1 mm mesh size whereas minimum one occurs 0.4 mm size.

Table 4. FEM Results in 1000 N - Quad4

| Force(N) | R | Element Shape | Element Size (mm) | Number of Element | Mesh Type | Mesh Method | Maximum Rooth Stres (Mpa) |
|---|---|---|---|---|---|---|---|
| 1000 | 60mm | Quad4 | 0,5mm | 2499 | Mixed | AutoDecide | 41,86 |
| | | | 0,4mm | 5786 | Mixed | AutoDecide | 41,63 |
| | | | 0,3mm | 7909 | Mixed | AutoDecide | 43,33 |
| | | | 0,2mm | 5548 | Mixed | Mapped | 43,69 |
| | | | 0,1mm | 10015 | Mixed | Mapped | 43,93 |
| | | | 0,05mm | 11605 | Mixed | Mapped | 43,70 |
| | | | 0,02mm | 40755 | Mixed | Mapped | 43,49 |
| | | | 0,01mm | 59938 | Mixed | Mapped | 43,45 |

The analysis result is given in Table 5 for 1000N and Quad8. Max gear tooth root stress is between 41,61Mpa and 48, 62 Mpa. Maximum stress is obtained for 0.4 mm mesh size whereas minimum one occurs 0.05 mm size.

Table 5. FEM Results in 1000 N – Quad8

| Force(N) | R | Element Shape | Element Size (mm) | Number of Element | Mesh Type | Mesh Method | Maximun Rooth Stre (Mpa) |
|---|---|---|---|---|---|---|---|
| 1000 | 60mm | Quad8 | 0,5mm | 2499 | Mixed | AutoDecide | 46,55 |
| | | | 0,4mm | 5786 | Mixed | AutoDecide | 48,62 |
| | | | 0,3mm | 7909 | Mixed | AutoDecide | 47,76 |
| | | | 0,2mm | 5548 | Mixed | Mapped | 43,73 |
| | | | 0,1mm | 10015 | Mixed | Mapped | 44,55 |
| | | | 0,05mm | 11605 | Mixed | Mapped | 43,61 |
| | | | 0,02mm | 40755 | Mixed | Mapped | 44,52 |
| | | | 0,01mm | 59938 | Mixed | Mapped | 43,65 |

The analysis result is given in Table 6 for 2000N and Quad4. Max gear tooth root stress is between 83,23Mpa and 87,84Mpa. Maximum stress is obtained for 0.1 mm mesh size whereas minimum one occurs 0.4 mm size.

Table 6. FEM Results in 2000 N - Quad4

| Force(N) | R | Element Shape | Element Size (mm) | Number of Element | Mesh Type | Mesh Method | Maximum Rooth Stres (Mpa) |
|---|---|---|---|---|---|---|---|
| **2000** | 60mm | Quad4 | 0,50 | 2499 | AutoDecide | Mapped | 83,70 |
| | | | 0,40 | 5786 | Mixed | Mapped | 83,23 |
| | | | 0,30 | 7909 | Mixed | Mapped | 86,63 |
| | | | 0,20 | 5548 | Mixed | Mapped | 87,36 |
| | | | 0,10 | 10015 | Mixed | Mapped | 87,84 |
| | | | 0,05 | 11605 | Mixed | Mapped | 87,38 |
| | | | 0,02 | 40755 | Mixed | Mapped | 86,96 |
| | | | 0,01 | 59938 | Mixed | Mapped | 86,87 |

The analysis result is given in Table 7 for 2000N and Quad8. Max gear tooth root stress is between 87,20Mpa and 97,22Mpa. Maximum stress is obtained for 0.4 mm mesh size whereas minimum one occurs 0.05 mm size.

Table 7. FEM Results in 2000 N – Quad8

| Force(N) | R | Element Shape | Element Size (mm) | Number of Element | Mesh Type | Mesh Method | Maximun Rooth Stre (Mpa) |
|---|---|---|---|---|---|---|---|
| 2000 | 60mm | Quad8 | 0,5mm | 2499 | Mixed | AutoDecide | 93,08 |
| | | | 0,4mm | 5786 | Mixed | AutoDecide | 97,22 |
| | | | 0,3mm | 7909 | Mixed | AutoDecide | 95,50 |
| | | | 0,2mm | 5548 | Mixed | Mapped | 87,43 |
| | | | 0,1mm | 10015 | Mixed | Mapped | 89,08 |
| | | | 0,05mm | 11605 | Mixed | Mapped | 87,20 |
| | | | 0,02mm | 40755 | Mixed | Mapped | 89,01 |
| | | | 0,01mm | 59938 | Mixed | Mapped | 87,28 |

The analysis result is given in Table 8 for 3000N and Quad4. Max gear tooth root stress is between 124,8Mpa and 131,7Mpa. Maximum stress is obtained for 0.1 mm mesh size whereas minimum one occurs 0.4 mm size.

Table 8. FEM Results in 3000 N – Quad4

| Force(N) | R | Element Shape | Element Size (mm) | Number of Element | Mesh Type | Mesh Method | Maximum Rooth Stres (Mpa) |
|---|---|---|---|---|---|---|---|
| 3000 | 60mm | Quad4 | 0,5mm | 2499 | Mixed | AutoDecide | 125,50 |
| | | | 0,4mm | 5786 | Mixed | AutoDecide | 124,80 |
| | | | 0,3mm | 7909 | Mixed | AutoDecide | 129,90 |
| | | | 0,2mm | 5548 | Mixed | Mapped | 131,00 |
| | | | 0,1mm | 10015 | Mixed | Mapped | 131,70 |
| | | | 0,05mm | 11605 | Mixed | Mapped | 131,00 |
| | | | 0,02mm | 40755 | Mixed | Mapped | 130,40 |
| | | | 0,01mm | 59938 | Mixed | Mapped | 130,30 |

The analysis result is given in Table 9 for 3000N and Quad8. Max gear tooth root stress is between 130,8 Mpa and 145,8 Mpa. Maximum stress is obtained for 0.4 mm mesh size whereas minimum one occurs 0.05 mm size.

Table 9. FEM Results in 3000 N – Quad8

| Force(N) | R | Element Shape | Element Size (mm) | Number of Element | Mesh Type | Mesh Method | Maximun Rooth Stre (Mpa) |
|---|---|---|---|---|---|---|---|
| 3000 | 60mm | Quad8 | 0,5mm | 2499 | Mixed | AutoDecide | 139,60 |
| | | | 0,4mm | 5786 | Mixed | AutoDecide | 145,80 |
| | | | 0,3mm | 7909 | Mixed | AutoDecide | 143,20 |
| | | | 0,2mm | 5548 | Mixed | Mapped | 131,10 |
| | | | 0,1mm | 10015 | Mixed | Mapped | 133,60 |
| | | | 0,05mm | 11605 | Mixed | Mapped | 130,80 |
| | | | 0,02mm | 40755 | Mixed | Mapped | 133,50 |
| | | | 0,01mm | 59938 | Mixed | Mapped | 130,90 |

The analysis result is given in Table 10 for 4000N and Quad4. Max gear tooth root stress is between 166,4Mpa and 175,6Mpa. Maximum stress is obtained for 0.1 mm mesh size whereas minimum one occurs 0.4 mm size.

Table 10. FEM Results in 4000 N – Quad4

| Force(N) | R | Element Shape | Element Size (mm) | Number of Element | Mesh Type | Mesh Method | Maximum Rooth Stres (Mpa) |
|---|---|---|---|---|---|---|---|
| 4000 | 60mm | Quad4 | 0,5mm | 2499 | Mixed | AutoDecide | 167,30 |
| | | | 0,4mm | 5786 | Mixed | AutoDecide | 166,40 |
| | | | 0,3mm | 7909 | Mixed | AutoDecide | 173,20 |
| | | | 0,2mm | 5548 | Mixed | Mapped | 174,60 |
| | | | 0,1mm | 10015 | Mixed | Mapped | 175,60 |
| | | | 0,05mm | 11605 | Mixed | Mapped | 174,70 |
| | | | 0,02mm | 40755 | Mixed | Mapped | 173,80 |
| | | | 0,01mm | 59938 | Mixed | Mapped | 173,70 |

The analysis result is given in Table 11 for 4000N and Quad8. Max gear tooth root stress is between 174,3Mpa and 194,4Mpa. Maximum stress is obtained for 0.4 mm mesh size whereas minimum one occurs 0.05 mm size.

Table 11. FEM Results in 4000 N – Quad8

| Force(N) | R | Element Shape | Element Size (mm) | Number of Element | Mesh Type | Mesh Method | Maximun Rooth Stre (Mpa) |
|---|---|---|---|---|---|---|---|
| 4000 | 60mm | Quad8 | 0,5mm | 2499 | Mixed | AutoDecide | 186,10 |
| | | | 0,4mm | 5786 | Mixed | AutoDecide | 194,40 |
| | | | 0,3mm | 7909 | Mixed | AutoDecide | 190,90 |
| | | | 0,2mm | 5548 | Mixed | Mapped | 174,80 |
| | | | 0,1mm | 10015 | Mixed | Mapped | 178,10 |
| | | | 0,05mm | 11605 | Mixed | Mapped | 174,30 |
| | | | 0,02mm | 40755 | Mixed | Mapped | 177,90 |
| | | | 0,01mm | 59938 | Mixed | Mapped | 174,50 |

The analysis result is given in Table 12 for 5000N and Quad4. Max gear tooth root stress is between 207,9Mpa and 219,5Mpa. Maximum stress is obtained for 0.1 mm mesh size whereas minimum one occurs 0.4 mm size.

Table 12. FEM Results in 5000 N – Quad4

| Force(N) | R | Element Shape | Element Size (mm) | Number of Element | Mesh Type | Mesh Method | Maximum Rooth Stre (Mpa) |
|---|---|---|---|---|---|---|---|
| 5000 | 60mm | Quad4 | 0,5mm | 2499 | Mixed | AutoDecide | 209,10 |
| | | | 0,4mm | 5786 | Mixed | AutoDecide | 207,90 |
| | | | 0,3mm | 7909 | Mixed | AutoDecide | 216,40 |
| | | | 0,2mm | 5548 | Mixed | Mapped | 218,20 |
| | | | 0,1mm | 10015 | Mixed | Mapped | 219,50 |
| | | | 0,05mm | 11605 | Mixed | Mapped | 218,30 |
| | | | 0,02mm | 40755 | Mixed | Mapped | 217,20 |
| | | | 0,01mm | 59938 | Mixed | Mapped | 217,00 |

The analysis result is given in Table 13 for 5000N and Quad8. Max gear tooth root stress is between 217,9Mpa and 242,9Mpa. Maximum stress is obtained for 0.4 mm mesh size whereas minimum one occurs 0.05 mm size.

Table 13. FEM Results in 5000 N – Quad8

| Force(N) | R | Element Shape | Element Size (mm) | Number of Element | Mesh Type | Mesh Method | Maximum Rooth Stre (Mpa) |
|---|---|---|---|---|---|---|---|
| 5000 | 60mm | Quad8 | 0,5mm | 2499 | Mixed | AutoDecide | 232,50 |
| | | | 0,4mm | 5786 | Mixed | AutoDecide | 242,90 |
| | | | 0,3mm | 7909 | Mixed | AutoDecide | 238,60 |
| | | | 0,2mm | 5548 | Mixed | Mapped | 218,40 |
| | | | 0,1mm | 10015 | Mixed | Mapped | 222,60 |
| | | | 0,05mm | 11605 | Mixed | Mapped | 217,90 |
| | | | 0,02mm | 40755 | Mixed | Mapped | 224,40 |
| | | | 0,01mm | 59938 | Mixed | Mapped | 218,10 |

## 2.4. Analytical Solution of Spur Gear Bending Stress

Calculation of tooth root stress of spur gear is based on Lewis equation and ISO Gear Standards. Spur gear strength is descripted (International Organization International Organization for Standardization 2006, Calculation of tooth bending strength) for Standardization 1982) Şahin, (2014) described the process in his master thesis. Equations are given below:

- The basic bending stress for gear teeth is obtained by using the Lewis formula

$$\sigma = \frac{F_t}{(b_a * m * Y)} \qquad (3)$$

F t = Tangential force on tooth
σ = Tooth Bending stress (MPa)
$b_a$ = Face width (mm)
Y = Lewis Form Factor
m = Module (mm)

- The Lewis formula is often expressed as

$$\sigma = \frac{F_t}{(b_a * p * y)} \qquad (4)$$

Where y = Y/π and p = circular pitch

You can find modified equation in ISO 6336-3 (ISO, 2009). According to analytical formulas, the results are presented in Table 14.

Table 14. Force versus Stress Values

| Force (N) | 1000 | 2000 | 3000 | 4000 | 5000 |
|---|---|---|---|---|---|
| Analytical Results (Mpa) | 44,89 | 89,78 | 134,67 | 179,56 | 224,46 |

Comparison of analytical and finite element results is presented in Figure 9- 13 for different mesh size. For different force values, analyses for Quad 4 are almost same. It can be said also for Quad 8. The closest result of finite element analysis to analytical calculation is obtained 0.1 mm mesh size for Quad 4 and Quad 8 whereas the value most far from analytical result is taken at 0.4 mm mesh size.

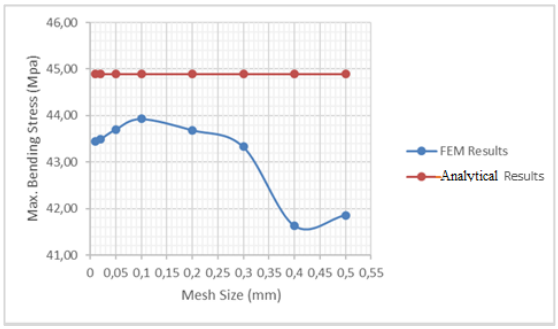


Fig. 9. Comparison of FEM Results and Analytical Solution for Quad4-1000N

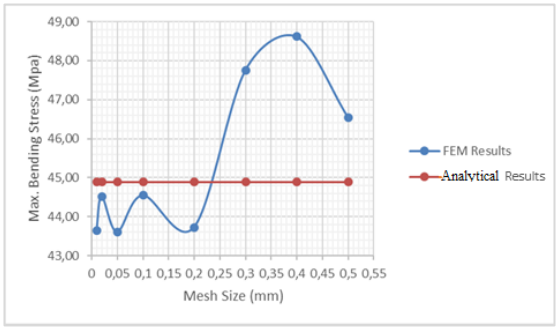


Fig. 11. Comparison of FEM Results and Analytical Solution for Quad8-1000N

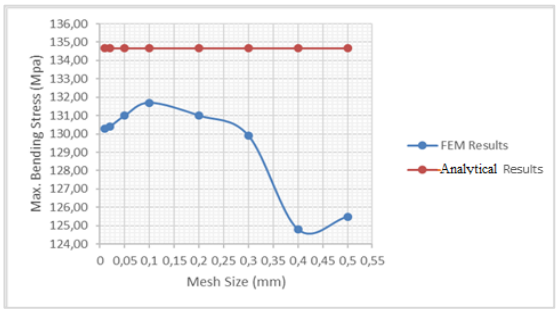


Fig. 12. Comparison of FEM Results and Analytical Solution for Quad4-3000N

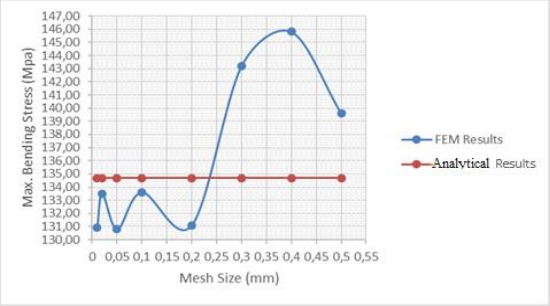


Fig. 13. Comparison of FEM Results and Analytical Solution for Quad8-3000N

The differences between finite element and analytical solutions' results is calculated according to following formulae:

$$\%\boldsymbol{E_r} = \left|\frac{\boldsymbol{R_a - R_{fem}}}{\boldsymbol{R_a}} * \mathbf{100}\right| \qquad (5)$$

Where Ra is analytical result, $R_{fem}$=FEM results and $E_r$=Error rate.

Error percent are obtained for Quad 4 and Quad 8, and then graphics is drawn. Minimum error for 0.1 mm and 0.02 mm mesh is observed as about 1% from Figure 19. Maximum error is observed for 0.4 mm mesh size as 8%.

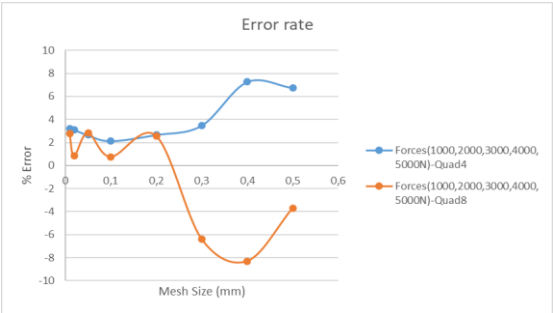


## 3. CONCLUSION

In this study, gear with 3 mm of module, 40 of teeth number and 20 degree of pressure angle is created by Catia. This gear model is meshed by Simxpert. Two different mesh types are used; Quad 4 and Quad 8. For this mesh models, 0.5 mm and 0.01 mm mesh sizes are used. Then five different loads (5000N, 4000N, 3000N, 2000N and 1000N) are applied by Marc. The results are presented in Tables3-Table12. Analytical calculations for gear tooth root stress are compared with Finite Element Analysis. According to results, Quad 8 mesh type and 0.1 mm mesh size are most suitable mesh parameters. 0.4 mm mesh size gives the most different results.

## REFERENCES

B. Sahin, (2014). "*Development of a user-friendly interface software for design and analysis of parallel axes external gears including quasi-static transmission error calculations*", Master thesis, University of Gaziantep, Gaziantep, Turkey.

International Organization for Standardization (2006), *Calculation of load capasity of spur and helical gears - Part3: Calculation of tooth bending strenght*, ISO 6336-3, International Organization for Standardization, Geneva.

MSC Softwares, *Cantilevered Plate*, http://www.mscsoftware.com/exercisemodules/cantilevered-plate [viewed 20 December 2015].

MSC Softwares, *Linear Analysis of a Cantilever Beam*, http://www.mscsoftware.com/exercisemodules/cantilevered-plate [viewed 10 March 2016].

O. Uctu. (2015). "*Design and Construction of a Parallel Axes Gear Research Test Rig*", Master thesis, University of Gaziantep, Gaziantep, Turkey.

P.B. Pawara, Abhay A. Utpatb. (2015). "*Analysis of Composite Material Spur Gear Under Static Loading Condition*", 4th International Conference on Materials Processing and Characterzation, Volume 2, Issues 4–5, Pages 2968–2974, India

V. Suresh Babu, A. A. Tsegaw. (2009). "*Involute Spur Gear Template Development by Parametric Technique Using Computer Aided*", An International Multi-Disciplinary Journal, Vol. 3 (2), Pp. 415-429, Ethiopia.

Zaigang Chena, Wanming Zhaia, Yimin Shaob, Kaiyun Wanga, Guohua Sunc. (2016). "*Analytical Model for Mesh Stiffness Calculation of Spur Gear Pair with Non-Uniformly Distributed Tooth Root Crack*", Engineering Failure Analysis, ISSN: 1350-6307, Republic of China

# CONTENTS




ISSN 2587-1366


# TURKISH JOURNAL OF ENGINEERING


VOLUME 1 ISSUE 1 MAY 2017